127.7, 126.9, 123.6, 115.1, 104.7, 102.5, 19.8. MS (EI *m/z*) 242 [M^+]. HRMS (EI *m/z*) calcd for $C_{15}H_{14}O_3$ [M]$^+$, 242.0943; found, 242.0944.

(*E*)-5-(4-Hydroxy-3,5-dimethylstyryl)benzene-1,3-diol (2). From **13b**. Yield, 68.6%; mp 205–208 °C. ^{1}H NMR (400 MHz, DMSO-d_6): δ 2.16 (6H, s), 6.09 (1H, dd, J = 2.0, 2.0 Hz), 6.35 (2H, d, J = 2.0 Hz), 6.74 (1H, d, J = 8.0 Hz), 6.78 (1H, d, J = 16.0 Hz), 6.84 (1H, d, J = 16.0 Hz), 7.13 (2H, s), 8.37 (1H, s), 9.19 (2H, s). ^{13}C NMR (100 MHz, DMSO-d_6): δ 160.4, 152.0, 138.8, 135.5, 129.6, 125.3, 122.2, 114.3, 105.1, 102.9, 16.5. MS (EI *m/z*) 256 [M^+]. HRMS (EI *m/z*) calcd for $C_{16}H_{16}O_3$ [M]$^+$, 256.10995; found, 256.10997.

(*E*)-5-(4-Hydroxystyryl)-2-methylbenzene-1,3-diol (4-Methylresveratrol). From **13c**. Yield, 59.8%; mp 239–242 °C. ^{1}H NMR (400 MHz, DMSO-d_6): δ 1.91 (3H, s), 6.43 (2H, s), 6.72 (2H, d, J = 8.8 Hz), 6.76 (2H, d, J = 16.4 Hz), 6.79 (1H, d, J = 16.4 Hz), 7.36 (1H, d, J = 8.8 Hz), 9.07 (2H, s), 9.51(1H, s). ^{13}C NMR (100 MHz, DMSO-d_6): δ 160.6, 158.7, 138.1, 131.5, 130.2, 128.5, 114.7, 110.5, 105.5, 9.8. MS (EI *m/z*) 242 [M^+]. HRMS (EI *m/z*) calcd for $C_{15}H_{14}O_3$ [M]$^+$, 242.0943; found, 242.0943.

(*E*)-5-(4-Hydroxy-3-methylstyryl)-2-methylbenzene-1,3-diol (3). From **13d**. Yield, 54.7%; mp 228–229 °C. ^{1}H NMR (400 MHz, DMSO-d_6): δ 1.91 (3H, s), 2.11 (3H, s), 6.42 (2H, s), 6.72 (1H, d, J = 8.4 Hz), 6.74 (1H, d, J = 16.4 Hz), 6.75 (1H, d, J = 16.4 Hz), 7.16 (1H, dd, J = 2.0, 8.0 Hz), 7.28 (1H, d, J = 2.0 Hz), 9.08 (2H, s), 9.40 (1H, s). ^{13}C NMR (100 MHz, DMSO-d_6): δ 161.6, 154.5, 138.8, 132.3, 129.8, 128.8, 127.0, 123.2, 116.9, 108.3, 104.1, 19.6, 9.4. MS (EI *m/z*) 256 [M^+]. HRMS (EI *m/z*) calcd for $C_{16}H_{16}O_3$ [M]$^+$, 256.10995; found, 256.10996.

(*E*)-5-(4-Hydroxy-3,5-dimethylstyryl)-2-methylbenzene-1,3-diol (4). From **13e**. Yield, 73.0%; mp 205–208 °C. ^{1}H NMR (400 MHz, DMSO-d_6): δ 1.91 (3H, s), 2.16 (6H, s), 6.43 (2H, s), 6.71 (1H, d, J = 16.4 Hz), 6.76 (1H, d, J = 16.4 Hz), 7.12 (2H, s), 8.33 (1H, s), 9.09 (2H, s). ^{13}C NMR (100 MHz, DMSO-d_6): δ 162.1, 158.2, 139.8, 132.6, 130.0, 128.4, 114.4, 109.5, 106.6, 9.8, −1.6. MS (EI *m/z*) 270 [M^+]. HRMS (EI *m/z*) calcd for $C_{16}H_{16}O_3$ [M]$^+$, 270.1256; found, 270.1259.

Spectral and Kinetic Measurements. Typically, an aliquot of methyl resveratrol (1.0×10^{-2} M) in deaerated MeCN was added to a quartz cuvette (10 mm i.d.) that contained galvinoxyl radical (G$^\bullet$) (2.5×10^{-6} M) in deaerated MeCN (3.0 mL). This led to a hydrogen transfer reaction from methyl resveratrol to G$^\bullet$. Changes in the UV–vis spectrum associated with this reaction were monitored using a Hewlett-Packard 8453 photodiode array spectrophotometer. The reaction rates were determined by following the change in absorbance at 428 nm due to G$^\bullet$ ($\epsilon = 1.43 \times 10^5$ M^{-1} cm^{-1}). Pseudofirst-order rate constants (k_{obs}) were determined by a least-squares curve fitting using an Apple Macintosh personal computer. The first-order plots of $\ln(A - A_\infty)$ vs time (A and $A\infty$ are denoted to the absorbance at the reaction time and the final absorbance, respectively) were linear until three or more half-lives, with the correlation coefficient $\rho > 0.999$.

ESR Measurement. An aliquot of deaerated MeCN solution of G$^\bullet$ (1.0×10^{-3} M) was added to a LABOTEC LLC-04B ESR sample tube containing deaerated MeCN solution of **4** (1.0×10^{-3} M), and ESR spectra of phenoxyl radical **4**$^\bullet$ produced in the reaction between **4** and G$^\bullet$ were taken on a JEOL X-band spectrometer (JES-FA100). The ESR spectrum was recorded under nonsaturating microwave power conditions. The magnitude of modulation was chosen to optimize the resolution and the signal-to-noise (S/N) ratio of the observed spectra. The g value and hyperfine coupling constants were calibrated with a Mn^{2+} marker. Computer simulation of the ESR spectra was carried out using Calleo ESR Version 1.2 program (Calleo Scientific Publisher) on an Apple Macintosh personal computer.

In Vitro CA Test. CHL cells were established from the lung of a female newborn Chinese hamster by Koyama et al. (*12*) and cloned by Ishidate and Odashima (*13*). They were maintained in Eagle's minimum essential medium (MEM; Gibco 11095-080) supplemented with 10% heat-inactivated fetal bovine serum and penicillin (100 U/mL)−streptomycin (100 μg/mL) (Gibco 15140-122) in 5% CO_2 in air at 37 °C. The doubling time was around 13 h, and the modal chromosome number was 25. Cells were seeded at 1.5×10^5/plate (60 mm in diameter) and incubated at 37 °C for 17 h. They were then treated with a test sample for 48 h, and colcemid (0.2 μg/mL) was added for the final 2 h. Chromosome preparations were made as follows: Cells were trypsinized and incubated in hypotonic KCl solution for 15 min and fixed three times with ice-cold fixative (glacial acetic acid:methanol, 1:3). Two drops of the fixed cell suspension were spread on a clean glass slide, air-dried, and stained with Giemsa solution. All slides were coded, and the number of cells with structural CAs was counted for 100 well-spread metaphases with a modal chromosome number of 25 ± 2.

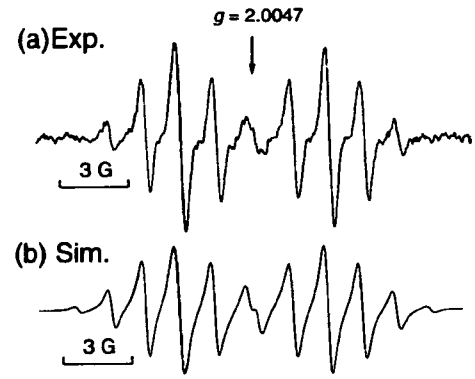

Figure 1. (a) ESR spectrum of phenoxyl radical generated in the reaction of **4** (5.0×10^{-4} M) with G$^\bullet$ (5.0×10^{-5} M) in deaerated MeCN at 298 K. (b) The computer simulation spectrum.

Table 1. Rate Constants (k_{HT}) of Hydrogen Transfer from Resveratrol and Methyl Analogues to G$^\bullet$

compd	k_{HT} (M^{-1} s^{-1})	compd	k_{HT} (M^{-1} s^{-1})
resveratrol	4.1	4-methylresveratrol	24.6
1	57.4	**3**	156
2	167	**4**	254

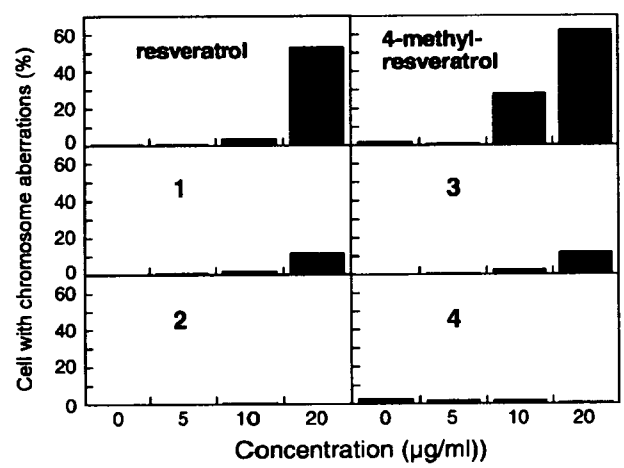

Figure 2. Chromosome aberrations induced in vitro by resveratrol and its methyl analogues. CHL cells were treated with the chemicals for 48 h.

Results and Discussion

Scheme 1 shows the structures of resveratrol and the designed methyl derivatives. Because the 4′-hydroxyl group is essential for both the antioxidative activity and the genotoxicity, resveratrol analogues were designed to introduce methyl groups ortho to the 4′-hydroxyl group. Methyl groups were also introduced at the 4-position para to the 4′-hydroxyl group. These

designed methyl derivatives (**1** and **2**) of resveratrol, 4-methylresveratrol, and its methyl derivatives (**3** and **4**) were synthesized by means of Wittig–Horner reactions between appropriate dibenzyloxybenzylphosphonic acid diethylesters (**5a,b**) and benzyloxybenzaldehydes (**6a–c**), followed by deprotection using $AlCl_3$ and *N,N*-dimethylaniline as outlined in Scheme 2. Trans geometries of these compounds were confirmed by their coupling constants (16.0–16.4 Hz) for the olefinic proton.

The radical scavenging activities of resveratrol and its analogues were evaluated by the hydrogen transfer reaction using galvinoxyl radical (G$^{\bullet}$) as an oxyl radical species. The hydrogen abstraction from resveratrols by G$^{\bullet}$ in deaerated acetonitrile was monitored by the decrease of absorbance at 428 nm due to G$^{\bullet}$ that obeyed pseudofirst-order kinetics, when the concentration of resveratrols was maintained at more than a 10-fold excess of the G$^{\bullet}$ concentration. The second-order rate constant (k_{HT}) for hydrogen abstraction was determined from the linear plot of pseudofirst-order rate constant vs the resveratrol concentration. As shown in Table 1, 3′-methylresveratrol (**1**), where one methyl group was introduced at the ortho position relative to the 4′-hydroxyl group, showed a significantly increased radical scavenging activity ascompared to resveratrol. A greater k_{HT} value was also obtained in compound **2**, which has methyl groups at both positions ortho to the 4′-hydroxyl group. In comparison to resveratrol, a 6-fold greater k_{HT} value was observed with 4-methylresveratrol, indicating that the 4-methyl group also affects the radical scavenging activities of the 4′-hydroxyl group. Similar to the methyl analogues (**1** and **2**) of resveratrol, the k_{HT} value of 4-methylresveratrol was increased by the introduction of methyl ortho to the 4′-hydroxyl group. Among resveratrol and its derivatives, compound **4** had the strongest antioxidative activity with a 60-fold greater k_{HT} value than that of resveratrol.

The strong antioxidative activity of tocopherol is attributed to the delocalization of phenoxyl radical, which is generated in the reaction with radical species, due to hyperconjugation with the *o*-methyl group (*11*). Therefore, to verify that the *o*-methyl group of **4** also contributes to delocalization of the unpaired electron in the corresponding phenoxyl radical, the ESR spectrum was measured for a solution containing **4** and G$^{\bullet}$ (Figure 1a). The observed ESR signals were characterized as the phenoxyl radical derived from **4** by computer simulation with the hyperfine splitting (hfs) values [$a_{CH_3}{}^{3'}$(3H), $a_{CH_3}{}^{5'}$(3H) = 0.141 mT, $a_H\alpha$(1H) = 0.601 mT] as shown in Figure 1b. We clearly demonstrated that the delocalization of the unpaired electron to the *o*-methyl groups by hyperconjugation results in the stronger antioxidative ability of *o*-methyl derivatives as compared to resveratrol.

We next considered the effect of the *o*-methyl group on the genotoxicity of resveratrol by means of the frequency of CA. Chinese hamster lung (CHL) cells were incubated with resveratrol and its analogues for 48 h, and the number of cells with structural CAs was counted after chromosome preparation. In agreement with a previous report (*8*), resveratrol induced a high frequency of CA consisting of obvious chromatid gaps and chromatid breaks. The frequency of CA is summarized in Figure 2. 4-Methylresveratrol showed a slightly higher frequency of CA as compared to resveratrol. Remarkably, *o*-methyl groups relative to 4′-hydroxyl group resulted in reduced genotoxicity. It is noteworthy that the frequency of CA induced by **1** and **3** was low, while CA induced by **2** and **4** was almost insignificant. These results suggest that two methyl substitutions reduce CA even more significantly than a single methyl substitution.

In conclusion, we have described the synthesis, antioxidative ability, and in vitro genotoxicity of resveratrol analogues with methyl groups ortho to the 4′-hydroxyl group. We demonstrated enhanced antioxidative activity coupled with reduced genotoxicity, rendering the methyl analogues **1–4** potentially valuable for the development of drugs effective for various types of diseases caused by oxidative stress. The genotoxicity of resveratrol has been attributed to the scavenging of tyrosyl free radicals in the R2 subunit of ribonucleotide reductase that catalyzes the rate-limiting step of de novo DNA synthesis (*14*). We previously reported that the 4′-hydroxyl group is responsible for scavenging tyrosyl radicals, which cause SCE and CA (*15*). Therefore, it is possible that the lower CA frequency for **1–4** as compared to resveratrol could be explained by the steric hindrance of the *o*-methyl group with respect to the radical scavenging reaction between the 4′-hydroxyl group and the tyrosyl radical. On the other hand, comparison of resveratrol and its *o*-methyl analogue (**1** and **2**) to the 4-methyl analogues (4-methyresveratrol, **3** and **4**), which have increased CA, shows a potential functional relationship between structure and enhanced radical scavenging activity. That is, slight increasing CA frequency in the corresponding 4-methyl analogues may be attributed to their enhanced radical scavenging activities that are responsible for theinhibition of ribonucleotide reductase. Further detailed insight and in vivo studies to fully exploit these potential benefits are currently underway.

Acknowledgment. This work was supported by a Grant from the Ministry of Health, Labour and Welfare, and by Grant-in-Aids for Scientific Research (B) (No. 17390033) and for Young Scientists (B) (No. 17790044) from the Ministry of Education, Culture, Sports, Science and Technology, Japan.

References

(1) Rotondo, S., Rajtar, G., Manarini, S., Celardo, A., Rotillo, D., de Gaetano, G., Evangelista, V., and Cerletti, C. (1998) Effect of trans-resveratrol, a natural polyphenolic compound, on human polymorphonuclear leukocyte function. *Br. J. Pharmacol. 123*, 1691–1699.

(2) Delmas, D., Jannin, B., and Latruffe, N. (2005) Resveratrol: Preventing properties against vascular alterations and ageing. *Mol. Nutr. Food Res. 49*, 377–395.

(3) Jang, M., Cai, L., Udeani, G. O., Slowing, K. V., Thomas, C. F., Beecher, C. W., Fong, H. H., Farnsworth, N. R., Kinghorn, A. D., Mehta, R. G., Moon, R. C., and Pezzuto, J. M. (1997) Cancer chemopreventive activity of resveratrol, a natural product derived from grapes. *Science 275*, 218–220.

(4) Fremont, L., Belguendouz, L., and Delpal, S. (1999) Antioxidant activity of resveratrol and alcohol-free wine polyphenols related to LDL oxidation and polyunsaturated fatty acids. *Life Sci. 64*, 2511–2521.

(5) Belguendouz, L., Fremont, L., and Linard, A. (1997) Resveratrol inhibits metal ion-dependent and independent peroxidation of porcine low-density lipoproteins. *Biochem. Pharmacol. 53*, 1347–1355.

(6) Stojanovic, S., Sprinz, H., and Brede, O. (2001) Efficiency and mechanism of the antioxidant action of trans-resveratrol and its analogues in the radical liposome oxidation. *Arch. Biochem. Biophys. 391*, 79–89.

(7) Fukuhara, K., Nagakawa, M., Nakanishi, I., Ohkubo, K., Imai, K., Urano, S., Fukuzumi, S., Ozawa, T., Ikota, N., Mochizuki, M., Miyata, N., and Okuda, H. (2006) Structural basis for DNA-cleaving activity of resveratrol in the presence of Cu(II). *Bioorg. Med. Chem. 14*, 1437–1443.

(8) Matsuoka, A., Furuta, A., Ozaki, M., Fukuhara, K., and Miyata, N. (2001) Resveratrol, a naturally occurring polyphenol, induces sister chromatid exchanges in a Chinese hamster lung (CHL) cell line. *Mutat. Res. 494*, 107–113.

(9) Matsuoka, A., Takeshita, K., Furuta, A., Ozaki, M., Fukuhara, K., and Miyata, N. (2002) The 4′-hydroxy group is responsible for the in vitro cytogenetic activity of resveratrol. *Mutat. Res. 521*, 29–35.

(10) Ovesna, Z., and Horvathova-Kozics, K. (2005) Structure-activity relationship of trans-resveratrol and its analogues. *Neoplasma 52*, 450–455.

(11) Nakanishi, I., Fukuhara, K., Shimada, T., Ohkubo, K., Iizuka, Y., Inami, K., Mochizuki, M., Urano, S., Itoh, S., Miyata, N., and Fukuzumi, S. (2002) Effects of magnesium ion on kinetic stability and spin distribution of phenoxy radical derived from a vitamin E analogue: Mechanistic insight into antioxidative hydrogen-transfer reaction of vitamin E. *J. Chem. Soc., Perkin Trans. 2*, 1520–1524.

(12) Koyama, H., Utakoji, T., and Ono, T. (1970) A new cell line derived from newborn Chinese hamster lung tissue. *Gann 61*, 161–167.

(13) Ishidate, M., Jr., and and Odashima, S. (1977) Chromosome tests with 134 compounds on Chinese hamster cells in vitro—A screening for chemical carcinogens. *Mutat. Res. 48*, 337–353.

(14) Fontecave, M., Lepoivre, M., Elleingand, E., Gerez, C., and Guittet, O. (1998) Resveratrol, a remarkable inhibitor of ribonucleotide reductase. *FEBS Lett. 421*, 277–279.

(15) Matsuoka, A., Lundin, C., Johansson, F., Sahlin, M., Fukuhara, K., Sjoberg, B. M., Jenssen, D., and Onfelt, A. (2004) Correlation of sister chromatid exchange formation through homologous recombination with ribonucleotide reductase inhibition. *Mutat. Res. 547*, 101–107.

TX7003008

Enhanced radical-scavenging activity of naturally-oriented artepillin C derivatives†

Sushma Manda,[a] Ikuo Nakanishi,*[ab] Kei Ohkubo,[b] Yoshihiro Uto,[c] Tomonori Kawashima,[b] Hitoshi Hori,[c] Kiyoshi Fukuhara,[d] Haruhiro Okuda,[d] Toshihiko Ozawa,[ae] Nobuo Ikota,[f] Shunichi Fukuzumi*[b] and Kazunori Anzai*[a]

Received (in Cambridge, UK) 16th October 2007, Accepted 14th November 2007
First published as an Advance Article on the web 28th November 2007
DOI: 10.1039/b715973k

More than two-fold augmentation in the radical-scavenging activity of artepillin C could be achieved *via* altering the O–H bond dissociation enthalpy of artepillin C by means of structural modifications.

Reactive oxygen species (ROS) and other free radicals have been implicated as pathological mediators in many clinical disorders. The reactivity of the most frequently encountered active free radicals, such as superoxide anion ($O_2^{\bullet -}$), hydroxyl radical ($^{\bullet}OH$), alkyl radical (R$^{\bullet}$), alkoxy radical (RO$^{\bullet}$), peroxyl radical (ROO$^{\bullet}$), nitric oxide (NO$^{\bullet}$) and lipid peroxyl radical (LOO$^{\bullet}$), varies, but some may cause severe damage to biological molecules, especially to DNA, lipids and proteins. However, several attempts including the use of naturally occurring and chemically synthesized antioxidants have been made to find out the possible ways for scavenging of these free radicals[1] and synthetic attempts have also been made in the last two decades to develop more potential antioxidants.[2] The plant-derived phenolic compounds have attracted much attention due to their limited or zero toxicity in *in vivo* systems. Artepillin C [3-{4-hydroxy-3,5-bis(3-methyl-2-butenyl)phenyl}-2(*E*)-propenoic acid] (**1H**), a major component (>5%) of Brazilian propolis,[3] has been reported to show antioxidative activity[4] alongside other important biological activities.[5] Recently, we reported the free radical-scavenging activity of artepillin C and also discussed the possible scavenging mechanism.[6] Since O–H bond dissociation enthalpy (D_{HT}) is known to regulate the antioxidative potency in phenolic compounds,[7] synthetic approaches towards the lowering of D_{HT} by structural modifications of artepillin C (**1H**) may result in remarkable changes in its antioxidative activity. We report herein the synthesis of five naturally-oriented artepillin C derivatives (**2H–6H**) (Scheme 1) and their enhanced scavenging activity towards cumylperoxyl radical (PhCMe$_2$OO$^{\bullet}$). PhCMe$_2$OO$^{\bullet}$, which is less reactive than RO$^{\bullet}$, is known to follow the same pattern of relative reactivity with a variety of substrates.[8] The structure–activity relationship is also discussed based on the results obtained in this study, providing a valuable insight into the development of antioxidants stronger than the naturally occurring ones.

Synthesis of **2H–6H** was based on regioselective *C*-prenylation of corresponding *ortho*-substituted phenols according to our established procedure[9] (see ESI,† S1). This indicates that the artepillin C derivatives could efficiently scavenge PhCMe$_2$OO$^{\bullet}$. In the presence of the artepillin C derivatives the decay rate of PhCMe$_2$OO$^{\bullet}$ follows pseudo-first-order kinetics. The pseudo-first-order rate constant (k) exhibits first-order dependence with respect to the concentration of the artepillin C derivatives. From the slopes of the linear plots were determined the second-order rate constants (k_{obs}) for the reaction between artepillin C derivatives and PhCMe$_2$OO$^{\bullet}$ in EtCN at 203 K. The k_{obs} value for the

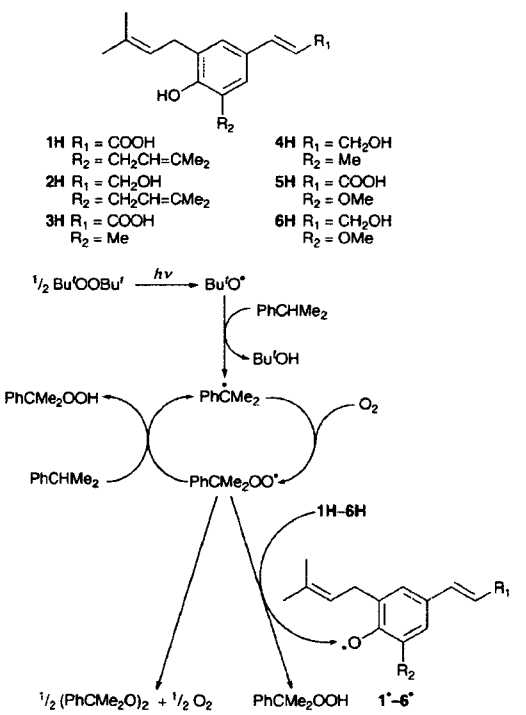

Scheme 1

[a]*Radiation Modifier Team, Heavy-Ion Radiobiology Research Group, Research Center for Charged Particle Therapy, National Institute of Radiological Sciences (NIRS), Inage-ku, Chiba 263-8555, Japan. E-mail: nakanis@nirs.go.jp; Fax: +81-43-255-6819; Tel: +81-43-206-3131*
[b]*Department of Material and Life Science, Graduate School of Engineering, Osaka University, SORST, Japan Science and Technology Agency (JST), Suita, Osaka 565-0871, Japan*
[c]*Faculty of Engineering, The University of Tokushima, Tokushima 770-8506, Japan*
[d]*Division of Organic Chemistry, National Institute of Health Sciences (NIHS), Setagaya-ku, Tokyo 158-8501, Japan*
[e]*Department of Health Pharmacy, Yokohama College of Pharmacy, Yokohama 245-0066, Japan*
[f]*School of Pharmacy, Shujitsu University, Okayama 703-8516, Japan*
† Electronic supplementary information (ESI) available: Detailed procedures for the synthesis of **2H–6H**. See DOI: 10.1039/b715973k

Table 1 Rate constants (k_{obs}) for scavenging of cumylperoxyl radical by **1H–6H** in EtCN at 203 K, energy difference values (D_{HT}) between phenoxyl radicals and phenols with reference to **1H**, and ionization potential (IP) values determined by density functional theory (DFT) calculations

Compound	k_{obs}/mol^{-1} dm^3 s^{-1}	D_{HT}/kcal mol^{-1}	IP/kcal mol^{-1}
1H	4.9×10^2	0	162.4
2H	5.7×10^2	−2.7	152.3
3H	1.5×10^2	0.5	164.9
4H	5.5×10^2	−2.1	154.3
5H	9.4×10^2	−4.2	162.3
6H	1.2×10^3	−6.0	153.2

$PhCMe_2OO^{\cdot}$ scavenging by **6H** (1.2×10^3 mol^{-1} dm^3 s^{-1}) is the largest among the examined artepillin C derivatives and is much larger than that for (+)-catechin (5.0×10^2 mol^{-1} dm^3 s^{-1}), which is one of the strongest antioxidants.[14,15] The rate constants of the $PhCMe_2OO^{\cdot}$-scavenging reactions by other derivatives have also been determined and are listed in Table 1. All the artepillin C derivatives, except **3H**, could afford significantly larger k_{obs} values than **1H** (4.9×10^2 mol^{-1} dm^3 s^{-1}). The k_{obs} value of **3H** was found to be smaller than that of **1H**, and this may be due to the absence of an electron-donating alkene group in **3H**. The k_{obs} value increases with an increasingly electron-rich environment in the molecule.

Direct measurements of the rate of the reaction between artepillin C derivatives and $PhCMe_2OO^{\cdot}$ were performed in propionitrile (EtCN) at 203 K by means of electron paramagnetic resonance (EPR). $PhCMe_2OO^{\cdot}$ is formed *via* a radical chain process as shown in Scheme 1.[10] The photoirradiation of Bu^tOOBu^t results in the homolytic cleavage of the O–O bond to produce $Bu^tO^{\cdot}$,[11] which abstracts a hydrogen atom from cumene to give cumyl radical, followed by the facile addition of molecular oxygen to cumyl radical. $PhCMe_2OO^{\cdot}$ can also abstract a hydrogen atom from cumene in the propagation step to yield cumene hydroperoxide, accompanied by regeneration of cumyl radical (Scheme 1).[12] In the termination step, $PhCMe_2OO^{\cdot}$ decays by a bimolecular reaction to yield the corresponding peroxide and molecular oxygen (Scheme 1).[13] In the presence of the artepillin C derivatives, the decay rate of $PhCMe_2OO^{\cdot}$ was much faster than that in their absence (Fig. 1).

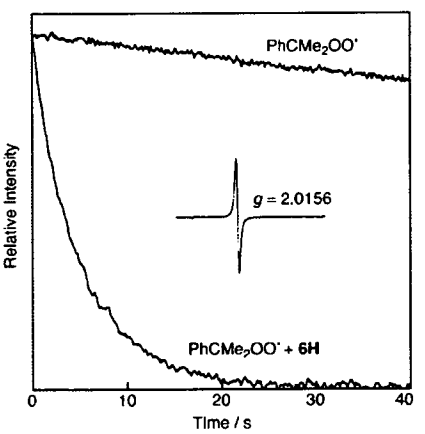

Fig. 1 Time course changes of the EPR signal intensity of $PhCMe_2OO^{\cdot}$ in the absence and presence of **6H** (1.3×10^{-4} mol dm^{-3}) in EtCN at 203 K. Inset: EPR spectrum of $PhCMe_2OO^{\cdot}$.

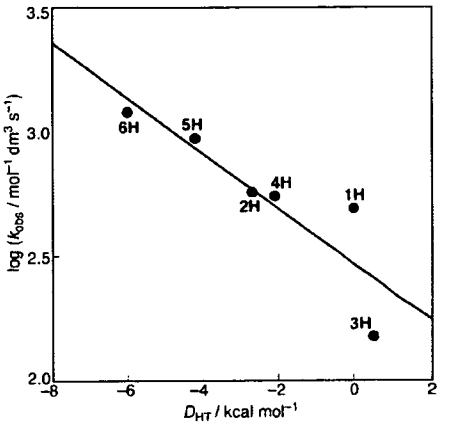

Fig. 2 Plot of log k_{obs} *vs.* calculated energy difference values (D_{HT}) between phenoxyl radicals and phenols with reference to **1H**.

It was also found that the k_{obs} values for the artepillin C derivatives were linearly correlated with the corresponding energy difference values, equal to D_{HT}, (Table 1) between the phenoxyl radicals (**1˙–6˙**) and the phenols determined by density functional theory (DFT) calculations[16] as shown in Fig. 2. On the other hand, as shown in Fig. 3, such a linear correlation cannot be observed between the k_{obs} values and the ionization potential (IP) calculated by DFT (Table 1). These results suggest that the $PhCMe_2OO^{\cdot}$-scavenging reaction by the artepillin C derivatives may proceed *via* a one-step hydrogen atom transfer rather than *via* an electron transfer oxidation of the artepillin C derivatives by $PhCMe_2OO^{\cdot}$.

Furthermore, enhancement in the antioxidative activity of the artepillin C derivatives can be explained by the fact that electron-donating (ED) groups reduce the D_{HT} and electron-withdrawing (EW) groups have the reverse effect.[17,18] By comparing the radical-scavenging efficiency of a series of artepillin C derivatives, we found the same trend and can conclude that the two structural factors are important for the antioxidative potency of the artepillin C derivatives, *i.e.*, the additional presence of ED substituents and the absence of EW groups. In fact, the k_{obs} value for **6H**, which is 2.4 times larger than that of **1H**, can be explained by the presence of two electron-donating groups, methoxy and hydroxypropenyl, in the molecule. Similarly, it can be explained why **3H** is least

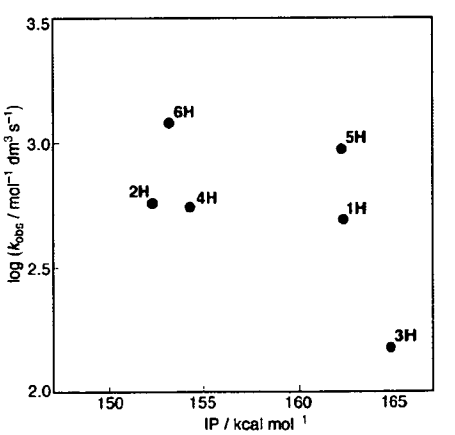

Fig. 3 Plot of log k_{obs} *vs.* calculated ionization potentials (IP) of **1H–6H**.

reactive followed by **1H**, **4H**, **2H**, **5H**, and **6H** among the examined artepillin C derivatives. By comparing the k_{obs} values for **1H–6H**, it is clear that the more electron-rich is the environment the compound has, the lower is its D_{HT} value, and the higher is its $PhCMe_2OO^{\bullet}$ scavenging activity.

In conclusion, structural modification of artepillin C, resulting in the decline of D_{HT}, leads to the enhancement of cumylperoxyl-scavenging activity. This is explained by the fact that **6H**, having six-fold lower D_{HT} as compared to artepillin C, showed more than two-fold higher $PhCMe_2OO^{\bullet}$-scavenging activity than artepillin C. Such an augmentation in radical-scavenging efficiency may have implications for reducing the excessive amount of radical scavenger used in *in vitro* as well as in *in vivo* studies.

This work was partially supported by Grant-in-Aid for Young Scientist (B) (Nos. 19790043 and 19750034) from the Ministry of Education, Culture, Sports, Science and Technology, Japan.

Notes and references

1 G. W. Burton and K. U. Ingold, *J. Am. Chem. Soc.*, 1981, **103**, 6472; V. R. Bowry and K. U. Ingold, *Acc. Chem. Res.*, 1999, **32**, 27; K. Hayashi, S. Komura, N. Isaji, N. Ohishi and K. Yagi, *Chem. Pharm. Bull.*, 1999, **47**, 1521; I. Nakanishi, Y. Uto, K. Ohkubo, K. Miyazaki, H. Yakumaru, S. Urano, H. Okuda, J. I. Ueda, T. Ozawa, K. Fukuhara, S. Fukuzumi, H. Nagasawa, H. Hori and N. Ikota, *Org. Biomol. Chem.*, 2003, **1**, 1452; N. Noguchi, Y. Iwaki, M. Takahashi, E. Komuro, Y. Kato, K. Tamura, O. Cynshi, T. Kodama and E. Niki, *Arch. Biochem. Biophys.*, 1997, **342**, 236.

2 M. Wijtmans, D. A. Pratt, L. Valgimigli, G. A. DiLabio, G. F. Pedulli and N. A. Porter, *Angew. Chem., Int. Ed.*, 2003, **42**, 4370; G. W. Burton, T. Doba, E. J. Gabe, L. Hughes, F. Lee, L. Prasad and K. U. Ingold, *J. Am. Chem. Soc.*, 1985, **107**, 7053; A. Watanabe, N. Noguchi, A. Fujisawa, T. Kodama, K. Tamura, O. Cynshi and E. Niki, *J. Am. Chem. Soc.*, 2000, **122**, 5438; D. A. Pratt, G. A. DiLabio, G. Brigati, G. F. Pedulli and L. Valgimigli, *J. Am. Chem. Soc.*, 2001, **123**, 4625; L. Valgimigli, G. Brigati, G. F. Pedulli, G. A. DiLabio, M. Mastragostino, C. Arbizzani and D. A. Pratt, *Chem.–Eur. J.*, 2003, **67**, 5190; M. C. Foti, E. R. Johnson, M. R. Vinqvist, J. S. Wright, L. R. C. Barclay and K. U. Ingold, *J. Org. Chem.*, 2002, **67**, 5190; K. Mukai, *Yukagaku*, 1991, **41**, 1063.

3 H. Aga, T. Shibuya, T. Sugimoto, S. Nakajima and M. Kurimoto, *Biosci., Biotechnol., Biochem.*, 1994, **58**, 945.

4 K. Hayashi, S. Komura, N. Isaji, N. Ohishi and K. Yagi, *Chem. Pharm. Bull.*, 1999, **47**, 1521.

5 T. Kimoto, S. Arai, M. Aga, T. Hanaya, M. Kohguchi, Y. Nomura and M. Kurimoto, *Gan to Kagaku Ryoho*, 1996, **23**, 1855; T. Matsuno, S. K. Jung, Y. Matsumoto, M. Saito and J. Morikawa, *Anticancer Res.*, 1997, **17**, 3565; Y. Nakajima, M. Shimazawa, S. Mishima and H. Hara, *Life Sci.*, 2006, **80**, 370; M. R. Ahn, K. Kunimasa, T. Ohta, S. Kumazawa, M. Kamihira, K. Kaji, Y. Uto, H. Hori, H. Nagasawa and T. Nakayama, *Cancer Lett.*, 2007, **252**, 235.

6 I. Nakanishi, Y. Uto, K. Ohkubo, K. Miyazaki, H. Yakumaru, S. Urano, H. Okuda, J. I. Ueda, T. Ozawa, K. Fukuhara, S. Fukuzumi, H. Nagasawa, H. Hori and N. Ikota, *Org. Biomol. Chem.*, 2003, **1**, 1452.

7 H. Y. Zhang, Y. M. Sun and X. L. Wang, *Chem.–Eur. J.*, 2003, **9**, 502; G. A. Russel, *Can. J. Chem.*, 1956, **34**, 1074; D. D. M. Wayner, E. Lusztyk, K. U. Ingold and P. Mulder, *J. Org. Chem.*, 1996, **61**, 6430; M. Lucarini, P. Pedrielli, G. F. Pedulli, S. Cabiddu and C. Fattuoni, *J. Org. Chem.*, 1996, **61**, 9263; G. Brigati, M. Lucarini, V. Mugnaini and G. F. Pedulli, *J. Org. Chem.*, 2002, **67**, 4828; H. Y. Zhang, Y. M. Sun and X. L. Wang, *Chem.–Eur. J.*, 2003, **9**, 502; G. A. Russel, *Can. J. Chem.*, 1956, **34**, 1074.

8 J. A. Howard, K. U. Ingold and M. Symonds, *Can. J. Chem.*, 1968, **46**, 1017.

9 Y. Uto, S. Ae, H. Nagasawa and H. Hori, *ACS Symp. Ser.*, 2005, **909**, 176.

10 R. A. Sheldon, in *The Activation of Dioxygen and Homogeneous Catalytic Oxidation*, ed. D. H. R. Barton, A. E. Martell and D. T. Sawyer, Plenum, New York and London, 1993, pp. 9–30; G. W. Parshall and S. D. Ittel, *Homogeneous Catalysis*, Wiley, New York, 2nd edn. 1992, ch. 10; A. E. Shilov, *Activation of Saturated Hydrocarbons by Transition Metal Complexes*, D. Reidel Publishing Co., Dordrecht, The Netherlands, 1984, ch. 4; A. Boettcher, E. R. Birnbaum, M. W. Day, H. B. Gray, M. W. Grinstaff and J. A. Labinger, *J. Mol. Catal. A: Chem.*, 1997, **117**, 229.

11 J. K. Kochi, *Free Radicals in Solution*, J. Wiley & Sons, New York, 1957; J. K. Kochi, P. J. Krusic and D. R. Eaton, *J. Am. Chem. Soc.*, 1969, **91**, 1877; P. J. Krusic and J. K. Kochi, *J. Am. Chem. Soc.*, 1969, **91**, 3938; P. J. Krusic and J. K. Kochi, *J. Am. Chem. Soc.*, 1969, **91**, 3942.

12 S. Fukuzumi and Y. Ono, *J. Chem. Soc., Perkin Trans. 2*, 1977, 622; S. Fukuzumi and Y. Ono, *J. Chem. Soc., Perkin Trans. 2*, 1977, 784.

13 J. A. Howard, *Adv. Free-Radical Chem. (London)*, 1972, **4**, 49.

14 I. Nakanishi, K. Miyazaki, T. Shimada, K. Ohkubo, S. Urano, N. Ikota, T. Ozawa, S. Fukuzumi and K. Fukuhara, *J. Phys. Chem. A*, 2002, **106**, 11123.

15 I. Nakanishi, K. Ohkubo, K. Miyazaki, W. Hakamata, S. Urano, T. Ozawa, H. Okuda, S. Fukuzumi, N. Ikota and K. Fukuhara, *Chem. Res. Toxicol.*, 2004, **17**, 26.

16 Density functional theory (DFT) calculations were performed on an 8CPU workstation (PQS, Quantum Cube QS8-2400C-064). Geometry optimizations were carried out using the Becke3LYP and 6-31G* basis set for the phenoxyl radical with the unrestricted Hartree–Fock (UHF) formalism as implemented in the Gaussian 03 program Revision C.02. The D_{HT} values were determined by the single point energy calculations at the B3LYP/6-31G* basis set with the restricted open shell Hartree–Fock (ROHF) formalism.

17 H. Y. Zhang, Y. M. Sun and X. L. Wang, *J. Org. Chem.*, 2002, **67**, 2709.

18 Y. M. Sun, H. Y. Zhang and D. Z. Chen, *Chin. J. Chem.*, 2001, **19**, 657.

Involvement of Electron Transfer in the Radical-scavenging Reaction of Resveratrol

Ikuo Nakanishi,*[1,2] Tomokazu Shimada,[3,4] Kei Ohkubo,[2] Sushma Manda,[1] Takehiko Shimizu,[3,4] Shiro Urano,[3] Haruhiro Okuda,[4] Naoki Miyata,[5] Toshihiko Ozawa,[1,6] Kazunori Anzai,[1] Shunichi Fukuzumi,[2] Nobuo Ikota,[7] and Kiyoshi Fukuhara*[4]

[1]*Radiation Modifier Team, Heavy-Ion Radiobiology Research Group, Research Center for Charged Particle Therapy, National Institute of Radiological Sciences (NIRS), Inage-ku, Chiba 263-8555*

[2]*Department of Material and Life Science, Graduate School of Engineering, Osaka University, SORST, Japan Science and Technology Agency (JST), Suita, Osaka 565-0871*

[3]*Department of Applied Chemistry, Shibaura Institute of Technology, Koto-ku, Tokyo 135-8548*

[4]*Division of Organic Chemistry, National Institute of Health Sciences (NIHS), Setagaya-ku, Tokyo 158-8501*

[5]*Graduate School of Pharmaceutical Sciences, Nagoya City University, Nagoya 467-8603*

[6]*Yokohama College of Pharmacy, Yokohama 245-0066*

[7]*School of Pharmacy, Shujitsu University, Okayama 703-8516*

(Received August 3, 2007; CL-070831; E-mail: nakanis@nirs.go.jp)

Resveratrol (3,4′,5-trihydroxy-*trans*-stilbene) efficiently scavenges an oxygen radical via an electron transfer from resveratrol to the radical in deaerated acetonitrile, which is significantly accelerated by the presence of magnesium ion.

Resveratrol (**1H**, 3,4′,5-trihydroxy-*trans*-stilbene), one of polyphenols found in grapes, has attracted considerable interest because of its antioxidative potential. **1H** has reported to inhibit the oxidation of human low-density lipoprotein (LDL) and reduce the propensity of human plasma and LDL to undergo lipid peroxidation.[1,2] Furthermore, it has been reported that **1H** inhibits cellular events associated with tumor initiation, promotion, and progression.[3] Besides its beneficial effects, **1H** was also shown to induce genotoxicity through a high frequency of micronucleus and sister chromatid exchange in vitro and DNA-cleaving activity in the presence of Cu^{II}.[4,5] However, very little is known about the detailed mechanism of antioxidative as well as toxic action of **1H**. On the other hand, two mechanisms are known for the antioxidative radical-scavenging reactions of polyphenols: a one-step hydrogen atom transfer from the phenolic OH group; and an electron transfer followed by a proton transfer.[6–8] Metal ions are a powerful tool that can be used to distinguish between these two mechanisms, since electron-transfer reactions are known to be significantly accelerated by their presence.[9] We report herein that the scavenging reaction of galvinoxyl radical (GO•), a relatively stable oxygen radical, by **1H** is significantly accelerated by the presence of magnesium ion in deaerated acetonitrile (MeCN). The detailed kinetic data obtained in this study provides valuable information about the antioxidative mechanism of **1H**, leading to the development of novel antioxidants with enhanced antioxidative abilities and reduced toxicity.

Upon addition of **1H** to a deaerated MeCN solution of GO•, the absorption band at 428 nm due to GO• disappeared immediately as shown in Figure 1. This spectral change suggests that **1H** can efficiently scavenge GO•. The rate of the GO•-scavenging reaction by **1H** was measured by monitoring the decrease in absorbance at 428 nm due to GO• using a photodiode array spectrophotometer. The decay of the absorbance at 428 nm due to GO• obeyed pseudo-first-order kinetics when the concentration of **1H** ([**1H**]) was maintained at more than a 10-fold excess of the GO•

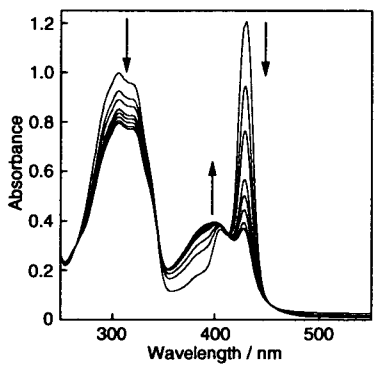

Figure 1. Spectral change observed in the reaction of **1H** (1.3×10^{-4} mol dm^{-3}) with GO• (8.0×10^{-6} mol dm^{-3}) in deaerated MeCN at 298 K (interval: 600 s).

concentration. The pseudo-first-order rate constants (k_{obs}) increase with increasing [**1H**], exhibiting first-order dependence on [**1H**]. From the slope of the linear plot of k_{obs} vs. [**1H**], the second-order rate constant (k) was determined for the radical-scavenging reaction as 4.1 dm^3 mol^{-1} s^{-1} in deaerated MeCN at 298 K. This k value is significantly smaller than those of representative natural phenolic antioxidants, such as (+)-catechin (2.6×10 dm^3 mol^{-1} s^{-1})[10] and a vitamin E model (3.0×10^3 dm^3 mol^{-1} s^{-1}).[11]

If the radical-scavenging reaction by **1H** involves an electron-transfer process as the rate-determining step, the rates of radical scavenging would be accelerated by the presence of metal ions.[12–14] This was investigated by examining the effect of $Mg(ClO_4)_2$ on the radical-scavenging rate by **1H** in deaerated MeCN. When $Mg(ClO_4)_2$ is added to the **1H**–GO• system in deaerated MeCN, the rate of GO•-scavenging reaction by **1H** was significantly accelerated. The k values increase linearly with increasing concentration of $Mg(ClO_4)_2$ as shown in Figure 2. It should be noted that there is no interaction between GO• and Mg^{2+}, since no spectral change was observed in the presence of a large amount of Mg^{2+}. Thus, the radical-scavenging reaction may proceed via an electron transfer from **1H** to GO•, which is accelerated by the presence of Mg^{2+}, followed by proton transfer from $\mathbf{1H}^{\bullet+}$ to GO^- as shown in Scheme 1. In such a case, the coordination of Mg^{2+} to GO^- may stabilize

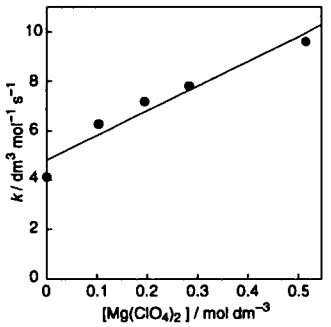

Figure 2. Dependence of k on $[Mg(ClO_4)_2]$ for the reaction of **1H** with GO$^\bullet$ in the presence of $Mg(ClO_4)_2$ in deaerated MeCN at 298 K.

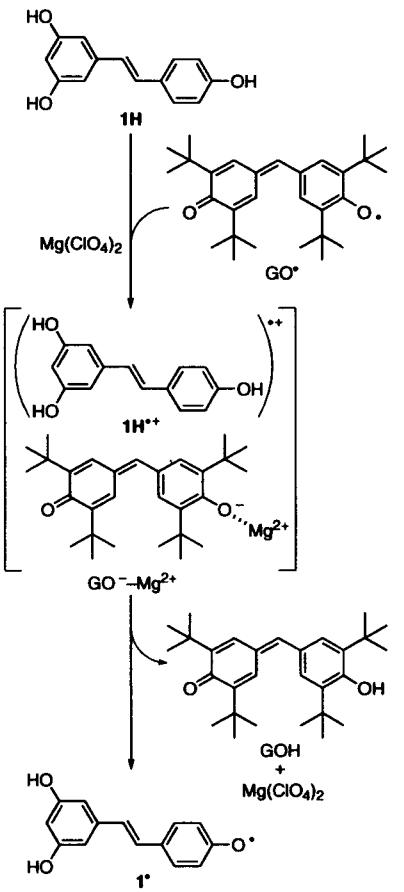

Scheme 1. Mg^{2+}-accelerated GO$^\bullet$-scavenging reaction by **1H** via an electron transfer.[15]

the product, resulting in the acceleration of the electron transfer (Scheme 1).[9,12–14] The one-electron oxidation potential (E^0_{ox} = 0.84 V vs. SCE) of **1H** determined by the second-harmonic alternating current voltammetry (SHACV)[16] in deaerated MeCN (0.1 M Bu_4NClO_4) is more positive than the one-electron reduction potential of GO$^\bullet$ (E^0_{red} = 0.05 V vs. SCE). This suggests that the reaction may involve a proton-coupled electron-transfer mechanism.[17]

In conclusion, resveratrol (**1H**) scavenges the oxygen radical via electron transfer in deaerated MeCN, which is accelerated by the presence of magnesium ion. The mechanistic information obtained in this study suggests that the introduction of electron-donating groups, such as methyl and methoxy groups, may stabilize the intermediate radical cation **1H**$^{\bullet+}$, resulting in the enhancement of the antioxidative abilities of **1H**. The synthesis of novel resveratrol derivatives having one or more methyl groups is currently under way and the results will be published in due time.

This work was partially supported by Grant-in-Aid for Young Scientist (B) (Nos. 19790043 and 19750034) from the Ministry of Education, Culture, Sports, Science and Technology, Japan.

References and Notes

1 E. N. Frankel, A. L. Waterhouse, J. E. Kinsella, *Lancet* **1993**, *341*, 1103.
2 L. Belguendouz, L. Fremont, A. Linard, *Biochem. Pharmacol.* **1997**, *53*, 1347.
3 M. Jang, L. Cai, G. O. Udeani, K. V. Slowing, C. F. Thomas, C. W. Beecher, H. H. Fong, N. R. Farnsworth, A. D. Kinghorn, R. G. Mehta, R. C. Moon, J. M. Pezzuto, *Science* **1997**, *275*, 218.
4 A. Matsuoka, K. Takeshita, A. Furuta, M. Ozaki, K. Fukuhara, N. Miyata, *Mutat. Res.* **2002**, *521*, 29.
5 K. Fukuhara, M. Nagakawa, I. Nakanishi, K. Ohkubo, K. Imai, S. Urano, S. Fukuzumi, T. Ozawa, N. Ikota, M. Mochizuki, N. Miyata, H. Okuda, *Bioorg. Med. Chem.* **2006**, *14*, 1437.
6 J. S. Wright, E. R. Johnson, G. A. DiLabio, *J. Am. Chem. Soc.* **2001**, *123*, 1173.
7 M. Leopoldini, T. Marino, N. Russo, M. Toscano, *J. Phys. Chem. A* **2004**, *108*, 4916.
8 M. Leopoldini, I. P. Pitarch, N. Russo, M. Toscano, *J. Phys. Chem. A* **2004**, *108*, 92.
9 S. Fukuzumi, in *Electron Transfer in Chemistry*, ed. by V. Balzani, Wiley-VCH, Weinheim, **2001**, Vol. 4, pp. 3–67.
10 I. Nakanishi, T. Kawashima, K. Fukuhra, H. Kanazawa, H. Okuda, S. Fukuzumi, T. Ozawa, N. Ikota, *ITE Lett. Batt. New Tech. Med.* **2004**, *5*, 585.
11 I. Nakanishi, K. Fukuhara, T. Shimada, K. Ohkubo, Y. Iizuka, K. Inami, M. Mochizuki, S. Urano, S. Itoh, N. Miyata, S. Fukuzumi, *J. Chem. Soc., Perkin Trans. 2* **2002**, 1520.
12 I. Nakanishi, K. Miyazaki, T. Shimada, K. Ohkubo, S. Urano, N. Ikota, T. Ozawa, S. Fukuzumi, K. Fukuhara, *J. Phys. Chem. A* **2002**, *106*, 11123.
13 I. Nakanishi, K. Ohkubo, K. Miyazaki, W. Hakamata, S. Urano, T. Ozawa, H. Okuda, S. Fukuzumi, N. Ikota, K. Fukuhara, *Chem. Res. Toxicol.* **2004**, *17*, 26.
14 I. Nakanishi, T. Kawashima, K. Ohkubo, H. Kanazawa, K. Inami, M. Mochizuki, K. Fukuhara, H. Okuda, T. Ozawa, S. Itoh, S. Fukuzumi, N. Ikota, *Org. Biomol. Chem.* **2005**, *3*, 626.
15 Although **1**$^\bullet$ could not be detected owing to follow-up radical reactions, density functional theory (DFT) calculations suggest that **1**$^\bullet$ may be the most stable among three possible phenoxyl radicals derived from **1H**; See: Ref. 5.
16 a) A. M. Bond, D. E. Smith, *Anal. Chem.* **1974**, *46*, 1946. b) E. M. Arnett, K. Amarnath, N. G. Harvey, J. Cheng, *J. Am. Chem. Soc.* **1990**, *112*, 344.
17 a) T. Osako, K. Ohkubo, M. Taki, Y. Tachi, S. Fukuzumi, S. Itoh, *J. Am. Chem. Soc.* **2003**, *125*, 11027. b) S. Fukuzumi, K. Ohkubo, Y. Tokuda, T. Suenobu, *J. Am. Chem. Soc.* **2000**, *122*, 4286.

Published on the web (Advance View) September 22, 2007; doi:10.1246/cl.2007.1276

Available online at www.sciencedirect.com
ScienceDirect
Bioorganic & Medicinal Chemistry
ELSEVIER
Bioorganic & Medicinal Chemistry 15 (2007) 3869–3873

9-Nitroanthracene derivative as a precursor of anthraquinone for photodynamic therapy

Kiyoshi Fukuhara,[a,*] Shinji Oikawa,[b] Nana Hakoda,[b] Yasunori Sakai,[c] Yusuke Hiraku,[b] Takuji Shoda,[a] Shinichi Saito,[c] Naoki Miyata,[d] Shosuke Kawanishi[b,e] and Haruhiro Okuda[a]

[a]*Division of Organic Chemistry, National Institute of Health Sciences, 1-18-1 Setagaya-ku, Tokyo 158-8501, Japan*
[b]*Department of Environmental and Molecular Medicine, Mie University Graduate School of Medicine, Tsu, Mie 514-8507, Japan*
[c]*Faculty of Science, Tokyo University of Science, Shinjuku-ku, Tokyo 162-8601, Japan*
[d]*Graduate School of Pharmaceutical Sciences, Nagoya City University, Mizuho-ku, Nagoya, Aichi 467-8603, Japan*
[e]*Faculty of Health Science, Suzuka University of Medical Science, Suzuka, Mie 510-0293, Japan*

Received 29 January 2007; revised 6 March 2007; accepted 7 March 2007
Available online 13 March 2007

Abstract—Anthraquinones are typical photosensitizers used in photodynamic therapy (PDT). However, systemic toxicity is a major problem for anthraquinones due to their ability not only to bind DNA but also to cause oxidative stress even without photoirradiation. To avoid such disadvantages in cancer therapy, we designed and synthesized a novel 9-nitroanthracene derivative (**1**) as a precursor of anthraquinone. Under photoirradiation, **1** is converted into anthraquinone via generation of nitric oxide as confirmed by ESR. Strong DNA cleavage specifically at guanine under photoirradiation was also observed, characteristic of DNA-cleaving reactions by photoirradiated anthraquinones. We propose development of **1** as an alternative approach toward PDT that reduces the systemic toxicity of anthraquinone.

1. Introduction

Photodynamic therapy (PDT) is an attractive approach to selectively localize toxicity using photosensitizers activated by light to induce cell death.[1,2] A large number of porphyrins have been tested for their efficacy in PDT, photofrin and photosan are currently in clinical use for PDT of lung cancer.[3,4] There is also considerable interest in understanding the factors contributing to the photodynamic activity of anthraquinones.[5–7] The ability of some anthraquinone derivatives to form cytotoxic reactive oxygen species (ROS) after illumination can result in effective ablation of targeted tissue. However, anthraquinones often carry complications of systemic toxicity as they tend to both bind DNA[8,9] and also cause oxidative stress even without photoirradiation.[10] Therefore, a prodrug of anthraquinone, which can be converted into anthraquinone only under photoirradiation, is required to overcome these disadvantages in cancer therapy. We have focused on the mechanism of photochemical degradation of 9-nitroanthracene to form anthraquinone via generation of nitric oxide (NO). A similar reaction is observed in 6-nitrobenzo[a]pyrene where the orientation of the nitro group is perpendicular to the aromatic ring due to the two protons located at the peri position, a similar situation for the nitro group in 9-nitroanthracene.[11] For 6-nitrobenzo[a]pyrene, three isomers of benzo[a]pyrenequinone are formed as a result of photodecomposition. If 9-nitroanthracene is used as a precursor of anthraquinone for PDT, complications of systemic toxicity can be avoided thereby benefiting its use in therapy. In this communication, we highlight a 9-nitroanthracene derivative (**1**) as a precursor of anthraquinone, an effective photosensitizer agent, and demonstrate its DNA cleaving activities under photoirradiation.

Keywords: Anthraquinone; 9-Nitroanthracene; Photodynamic therapy; DNA cleavage.
* Corresponding author. Tel.: +81 3 3700 1141; fax: +81 3 3707 6950; e-mail: fukuhara@nihs.go.jp

0968-0896/$ - see front matter © 2007 Elsevier Ltd. All rights reserved.
doi:10.1016/j.bmc.2007.03.029

2. Results and discussion

For the purpose of PDT, **1** was designed to have a dimethyl aminoalkyl group at the 2-position of 9-nitroanthracene. This group should increase solubility and DNA-binding affinity compared to 9-nitroanthracene itself. The synthesis of **1** and its isomer (**2**) with a nitro group at the 1-position is described in Scheme 1. 2-Aminoanthracene was condensed with 4-dimethylaminobutylic acid to give the dimethylaminoalkyl derivative at 87% yield. Nitration of the derivative with HNO_3 in acetic anhydride proceeded at 1- and 9-positions to give compounds **2** and **1** at 25% and 58% yields, respectively.

Comparing the stabilities of **1** and **2** under photoirradiation, **1** was much more susceptible to decomposition than **2**, consistent with the fact that **1** is almost completely decomposed 3 hours later, while photodegradation of **2** is not observed under the same conditions as shown in Figure 1a. Product analysis after photolysis of **1** showed that anthraquinone derivative (AQ) was formed at 77% yield, the structure of which was confirmed by ^1H NMR and mass spectrometry. It is likely that photolabile **1** releases NO in the course of anthraquinone formation. To assess the generation of NO upon photoirradiation, an ESR experiment with (MGD)-Fe^{2+} as the spin trap[12] was performed. As shown in Figure 1b, a three-line spectrum consistent of $a^N = 1.25$ mT and $g^{iso} = 2.04$, characteristic of the [$(MGD)_2$-Fe^{2+}-NO] complex, was observed from photoirradiated **1**, indicating that degradation of photolabile **1** is accompanied by generation of NO. In contrast, we could barely observe a similar peak in the case of photostable **2**. These results show that **1** is a promising photosensitizer that is converted into an AQ structure under photoirradiation via a NO-releasing mechanism.

Photosensitizers are activated by light to induce cell death or modulation of immunological cascades, presumably via formation of ROS. Therefore, the abilities of **1** and **2** to cleave DNA were examined by agarose gel electrophoresis of pBR322DNA. As shown in Figure 2a, no effect of **1** and **2** on DNA was observed in the dark condition. When irradiation was performed for 30 min, **1** induced efficient strand cleavage as shown in Figure 2b, and in the presence of 200 μM **1**, almost all

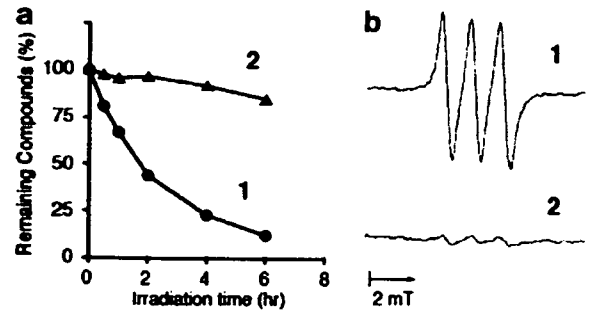

Figure 1. Photodegradation of **1** and **2**, and generation of NO. (a) Remaining **1** and **2** after photodegradation. (b) ESR spectra of (MGD)-Fe^{2+} in the presence of **1** and **2** after photoirradiation for 6 min.

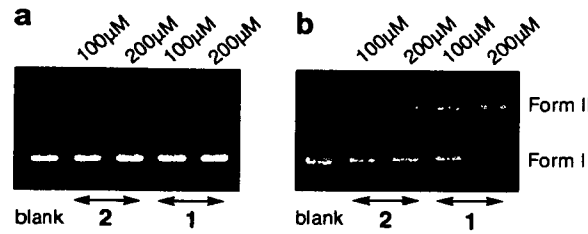

Figure 2. Effects of **1** and **2** on supercoiled pBR322DNA in the dark (a) or under photoirradiation (b).

of Form I (supercoiled) DNA was converted to Form II (closed circular) DNA. In contrast, although strand scission by **2** was obviously observed, the DNA-cleaving ability was not so strong compared with that of **1**. The strong DNA cleavage induced by **1** might be triggered by a structural change in AQ under photoirradiation. To confirm the generation of $^1O_2$ under photoirradiation, ESR spectra were observed in the presence of 2,2,6,6-tetramethyl-4-piperidone (4-oxo-TEMP), a spin trap for $^1O_2$. As shown in Figure 3, a three-line spectrum consistent of $a^N = 1.60$ mT, which is characteristic of 4-oxo-TEMPO,[13] was observed from both **1** and **2**, indicating generation of $^1O_2$. Importantly, the ability of **1** to generate $^1O_2$ as reflected in the peak height of 4-oxo-TEMPO was stronger than that for **2**, demonstrating

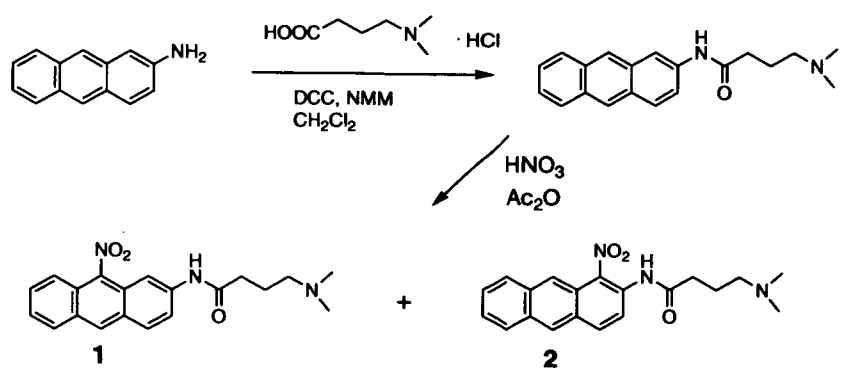

Scheme 1. Structures of **1** and **2**, and their synthesis.

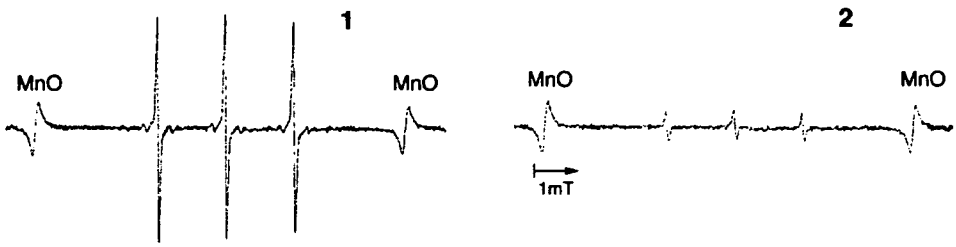

Figure 3. ESR spectra of 4-oxo-TEMP in the presence of 1 and 2 after photoirradiation for 10 min.

the advantage of **1** in cleaving DNA after conversion into AQ.

Photoexcited AQ (AQ^{3*}) is responsible for DNA damage through electron transfer from the DNA base (Type I mechanism)[14] or by generation of ROS such as $^1O_2$ (Type II mechanism).[15] Both mechanisms would result in DNA strand scission primarily at guanines. Therefore, photocleavage experiments induced by **1** were also performed with 5′-^{32}P-end labeled oligonucleotides to test targeting of specific cleaving sites. As expected, irradiation of DNA in the presence of **1** for 30 min and subsequent treatment with piperidine revealed that strand cleavage occurs predominantly at guanine, as shown in Figure 4.

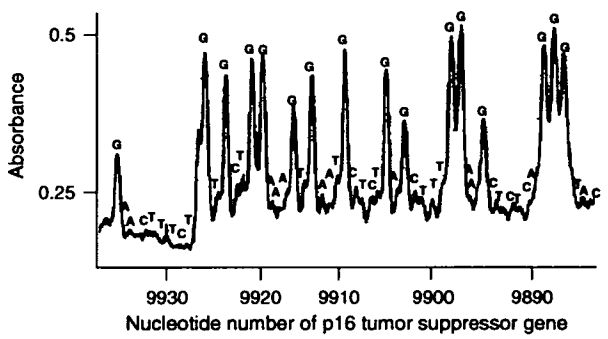

Figure 4. Sequence specificity of DNA damage in the p16 tumor suppressor gene, induced by **1** upon photoirradiation.

In summary, we have described the design and synthesis of **1** as a precursor of anthraquinone, a typical photosensitizer. Photochemical conversion of **1** into anthraquinone via generation of NO and specific DNA cleavage at guanine were demonstrated, characteristic of DNA-cleaving reactions of anthraquinones. A possible mechanism of oxidative DNA cleavage induced by photoirradiated **1** is shown in Scheme 2. The perpendicular conformation of the nitro group to the anthracene is characteristic for **1** and is responsible for the ease of NO generation which is followed by structural conversion into anthraquinone.[16] That is, the perpendicular conformation of nitro group in **1** suggests that the overlap of half-vacant nonbonding orbital of the nitro group with the adjacent orbital of the aromatic ring increases susceptibility to intramolecular rearrangement from nitro to nitrite. In comparison, such rearrangement does not occur in the case of **2** where the conformation of nitro group is not perpendicular (data not shown). There are a number of nitro polycyclic aromatic hydrocarbons (nitroPAHs) showing mutagenicity and/or carcinogenicity. However, no such toxicity has been shown by 9-nitroanthracene because the nitro group at 9-position is insensitive to enzymatic reduction, essential

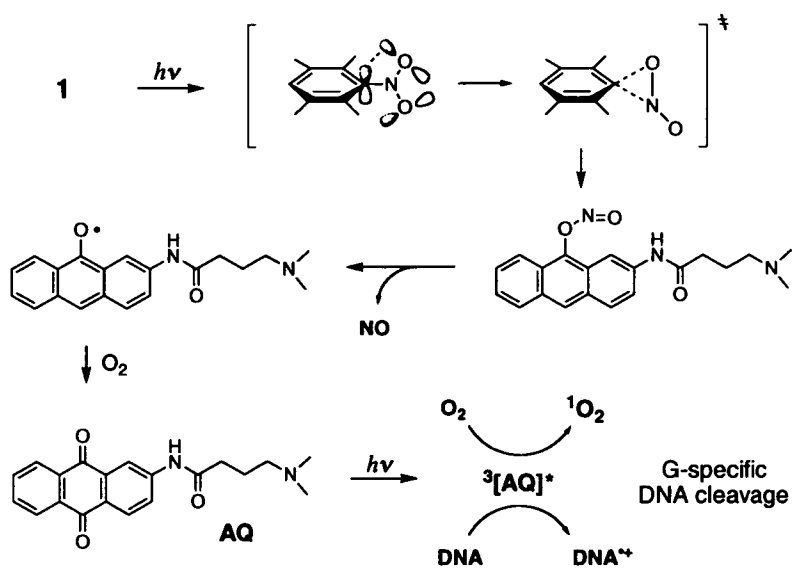

Scheme 2. Possible mechanism of oxidative DNA damage induced by photoirradiated **1**.

for the toxicity of nitroPAH.[17] Interestingly, two peri protons at the 1- and 8-positions, which lead to a perpendicular conformation of the nitro group, impede access of reductase to 9-nitroanthracene.[17,18] Finally, **1** might be favorable for PDT as an approach to reducing the systemic toxicity of anthraquinone. Further investigation to understand the mechanism of DNA cleaving activity and apoptotic cell death induced by **1** is underway and will be reported in due course.

3. Experimental

3.1. General methods

The reagents and solvents used were of commercial origin (Wako chemicals, Sigma, Aldrich) and were employed without further purification. The progress of all reactions was monitored by thin-layer chromatography on silica gel 60 F_{254} (0.25 mm, Merck). Column chromatography was performed on silica gel 60 (0.063–0.200 mm, Merck). The ^1H NMR spectra were recorded with a Varian AS 400 Mercury spectrometer. Chemical shifts were expressed in ppm downfield shift from Me_4Si. High resolution mass spectra were obtained on a JEOL MS700 mass spectrometer. ESR spectra were obtained with a JEOL X-band spectrometer (JES-FA100) under nonsaturating microwave power conditions.

3.2. Synthesis of *N*-(anthracen-2-yl)-4-(dimethylamino)butanamide (3)

To a solution of 2-aminoanthracene (580 mg, 3 mmol) and *N*-methylmorpholine (303 mg, 3 mmol) in DMF (10 ml) were added 4-(dimethylamino)butyric acid hydrochloride (503 mg, 3 mmol) and *N*-methylmorpholine (303 mg, 3 mmol) in DMF (10 ml) at 0 °C and the mixture was stirred for 18 h. After removal of the solvent in vacuo, the residue was dissolved in CH_2Cl_2 and filtered. The filtrate was washed with saturated NaCl, dried over anhydrous Na_2SO_4, and concentrated in vacuo. The residue was purified by silica gel column chromatography (CH_2Cl_2/MeOH/Satd NH_3 in MeOH, 100:20:1) to afford the title compound (796 mg, 87%) as a white solid. ^{1}HMR ($CDCl_3$, 400 MHz) δ 1.95 (2H, m), 2.40 (6H, s), 2.54 (2H, m), 2.61 (2H, m), 7.38 (1H, d, J = 9.2 Hz), 7.43 (2H, m), 7.94 (1H, d, J = 8.8 Hz), 7.95 (1H, d, J = 7.6 Hz), 7.96 (1H, d, J = 9.2 Hz), 8.34 (1H, s), 8.35 (1H, s), 8.47 (1H, s), 10.11(1H, br); HR-MS (+EI) $(M)^+$ found 306.1731; $(M)^+$ calcd for $C_{20}H_{22}N_2O$ 306.1734.

3.3. Synthesis of 4-(dimethylamino)-*N*-(9-nitroanthracen-2-yl)butanamide (1) and 4-(dimethylamino)-*N*-(1-nitroanthracen-2-yl)butanamide (2)

To a suspension of **1** (238 mg, 0.78 mmol) in acetic anhydride (35 mL) was added HNO_3 (0.17 mL) in acetic acid (1.8 mL) dropwise over 10 min at −10 °C. After stirring at 0 °C for 20 min, the mixture was poured onto crushed ice and stirred for 2 h, extracted with CH_2Cl_2, and the extracts were washed with H_2O and brine, dried over anhydrous Na_2SO_4, and concentrated in vacuo. The residue was purified by silica gel column chromatography (benzene/ethyl acetate/MeOH/Satd NH_3 in MeOH, 40:40:15:5) to afford **2** and **1** in this order as a light orange solid.

1. 159 mg, 58% yield, UV λ_{max} (MeOH) nm: 224, 260, 364; ^{1}HMR ($CDCl_3$, 400 MHz) δ 1.93 (2H, m), 2.43 (6H, s), 2.57 (2H, m), 2.62 (2H, m), 7.51 (1H, m), 7.63 (1H, m), 7.89 (1H, s), 7.93 (1H, d, J = 8.8 Hz), 8.02 (1H, d, J = 9.1 Hz), 8.03 (1H, d, J = 8.4 Hz), 8.09 (1H, d, J = 9.1 Hz), 8.54 (1H, s), 11.22 (1H, br); HR-MS (+EI) $(M)^+$ found 351.1585; $(M)^+$ calcd for $C_{20}H_{21}N_3O_3$ 351.1584.

2. 68 mg, 25% yield, UV λ_{max} (MeOH) nm: 241, 269, 379; ^{1}HMR ($CDCl_3$, 400 MHz) δ 1.96 (2H, m), 2.32 (6H, s), 2.49 (2H, m), 2.61 (2H, m), 7.55 (2H, m), 8.01 (2H, m), 8.15 (1H, d, J = 9.4 Hz), 8.29 (1H, d, J = 9.4 Hz), 8.45 (1H, s), 8.62 (1H, s), 10.20 (1H, br); HR-MS (+EI) $(M)^+$ found 351.1581; $(M)^+$ calcd for $C_{20}H_{21}N_3O_3$ 351.1584.

3.4. Photolysis of 1

A 3.5 mg (0.01 mmol) of **1** was dissolved in 4 ml of benzene/acetone (1:1) and irradiation was performed through a Pyrex filter with a 300W photoreflector lamp for 3 h. The reaction mixture was concentrated in vacuo and purified by silica gel column chromatography (benzene/ethyl acetate/MeOH/Satd NH_3 in MeOH, 40:45:10:5) to afford 4-(dimethylamino)-*N*-(9,10-dioxo-9,10-dihydroanthracen-2-yl)butanamide (AQ) as a pale yellow solid (2.6 mg, 77% yield). UV λ_{max} (MeOH) nm: 219, 272, 356; ^{1}HMR ($CDCl_3$, 400 MHz) δ 2.29 (2H, m), 2.89 (6H, s), 2.94 (2H, m), 3.18 (2H, m), 7.97 (2H, m), 8.10 (1H, d, J = 8.8 Hz), 8.21 (1H, d, J = .8 Hz), 8.26 (1H, d, J = 8.0 Hz), 8.29 (1H, d, J = 8.0 Hz), 8.61 (1H, s), 10.33 (1H, br); HR-MS (+EI) $(M)^+$ found 336.1476; $(M)^+$ calcd for $C_{20}H_{20}N_2O_3$ 336.1475.

3.5. Detection of nitric oxide and $^1O_2$ by ESR

The Fe^{2+} complex of MGD [Fe^{2+}-MGD_2, (Fe-MGD)] was used to trap NO. Fresh stock solutions of Fe-MGD (1:5) were prepared by adding ferrous ammonium sulfate to an aqueous solution of MGD. A sample containing 200 μM of **1** or **2** and 15 mM MGD-Fe in phosphate buffer, pH 7.6 (5% DMF) was introduced into a quartz flat cell. ESR spectra were recorded after light irradiation (5 J/cm^2 UVA) at 30 cm distance with a JES-FE 2XG spectrometer (JEOL Co. Ltd., Tokyo, Japan). The spectrometer settings used were: modulation frequency, 100 kHz; amplitude, 100–1000; scan time, 4 min; microwave power, 16 mW; microwave frequency, 9.394 GHz. Detection of $^1O_2$ was performed by ESR using 2,2,6,6-tetramethyl-4-piperidone (4-oxo-TEMP) as a spin trap. A sample containing 100 μM of **1** or **2** and 100 mM of TEMP in phosphate buffer, pH 7.4 (5% DMF) was introduced into a quartz flat cell. ESR spectra were recorded in a similar manner as above.

3.6. Assays for DNA strand breaks

DNA strand breakage was measured by the conversion of supercoiled pBR322 plasmid DNA to the open circular form. Reactions were carried out in 20 μL (total volume) of 50 mM Na cacodylate buffer (5% DMF), pH 7.2, containing 45 μM of pBR322 DNA and 100 and 200 μM of **1** and **2**. The mixture was exposed to 5 J/cm^2 UVA light on ice using a 10 W UV lamp (365 nm, UVP, Inc., CA, USA) placed at a distance of 20 cm. After 30 min, the reaction mixtures were treated with 5 μL of loading buffer (100 mM TBE buffer, pH 8.3, containing 30% glycerol, 0.1% bromophenol blue) and applied to a 1% agarose gel. Horizontal gel electrophoresis was carried out in 50 mM TBE buffer, pH 8.3, and gels were stained with ethidium bromide (1 μg/ml) for 30 min, followed by destaining in water for 30 min and photography with UV translumination.

3.7. Site specificity of DNA damage induced by 1

3.7.1. Preparation of ^{32}P-5′-end-labeled DNA fragments. DNA fragments were obtained from the human p16 tumor suppressor genes. The ^{32}P-3′-end-labeled 460-base pair fragment (*Eco*RI*9481–*Eco*RI*9940) containing exon 2 of the human p16 tumor suppressor gene was obtained as previously described.[19] The 460-bp fragment was further digested with *Bss*HII to obtain the singly labeled 309-base pair (*Bss*HII 9789–*Eco*RI*9481) and 147-base pair (BssHII*9794–*Eco*RI*9940) DNA fragments.[20] An asterisk indicates ^{32}P labeling.

3.7.2. Detection of DNA damage induced by UVA in the presence of 1. The standard reaction mixture in a microtube (1.5-ml Eppendorf) contained a ^{32}P-labeled DNA fragment, 5 μM calf thymus DNA, and **1** in 10 mM sodium phosphate buffer (pH 7.8) containing 5 μM DTPA. The mixture was exposed to 5 J/cm^2 UVA light on ice using a 10 W UV lamp (365 nm, UVP, Inc., CA, USA) placed at a distance of 10 cm. After irradiation, the DNA fragments were treated for 20 min at 90 °C in 1 M piperidine and then electrophoresed on an 8% polyacrylamide/8 M urea gel. The autoradiogram was obtained by exposing an X-ray film to the gel. The preferred cleavage sites were determined by direct comparison of the position of the oligonucleotides with those produced by the chemical reactions of Maxam–Gilbert procedure using a DNA sequencing system (LKB2010 Macrophor). The relative amounts of oligonucleotides from treated DNA fragments were measured with a laser densitometer (LKB 2222 UltroScan XL).

Acknowledgments

This work was supported partly by a Grant from the Ministry of Health, Labour and Welfare, and by a Grant-in-Aid for Research of Health Sciences focusing on Drug Innovation (KH51058) from the Japan Health Sciences Foundation, partly by Grant-in-Aid for Scientific Research (B) (No. 17390033) from the Ministry of Education, Culture, Sports, Science and Technology, Japan.

References and notes

1. Dougherty, T. J. *Photochemically Activated Anticancer Agents*; American Chemical Society: Washington, DC, 1995.
2. Dalla Via, L.; Marciani Magno, S. *Curr. Med. Chem.* **2001**, *8*, 1405–1418.
3. Fisher, A. M.; Murphree, A. L.; Gomer, C. J. *Lasers Surg. Med.* **1995**, *17*, 2–31.
4. Boyle, R. W.; Dolphin, D. *Photochem. Photobiol.* **1996**, *64*, 469–485.
5. Diwu, Z.; Lown, J. W. *Pharmacol. Ther.* **1994**, *63*, 1–35.
6. Andreoni, A.; Colasanti, A.; Malatesta, V.; Riccio, P.; Roberti, G. *Photochem. Photobiol.* **1991**, *53*, 797–805.
7. Johnson Inbaraj, J.; Krishna, M. C.; Gandhidasan, R.; Murugesan, R. *Biochim. Biophys. Acta* **1999**, *1472*, 462–470.
8. McKnight, R. E.; Zhang, J.; Dixon, D. W. *Bioorg. Med. Chem. Lett.* **2004**, *14*, 401–404.
9. Chou, K. M.; Krapcho, A. P.; Horn, D.; Hacker, M. *Biochem. Pharmacol.* **2002**, *63*, 1143–1147.
10. Venditti, P.; Balestrieri, M.; De Leo, T.; Di Meo, S. *Cardiovasc. Res.* **1998**, *38*, 695–702.
11. Fukuhara, K.; Kurihara, M.; Miyata, N. J. *Am. Chem. Soc.* **2001**, *123*, 8662–8666.
12. Komarov, A.; Mattson, D.; Jones, M. M.; Singh, P. K.; Lai, C. S. *Biochem. Biophys. Res. Commun.* **1993**, *195*, 1191–1198.
13. Moan, J.; Wold, E. *Nature* **1979**, *279*, 450–451.
14. Breslin, D. T.; Schuster, G. B. *J. Am. Chem. Soc.* **1996**, *118*, 2311–2319.
15. Reszka, K. J.; Bilski, P.; Chignell, C. F.; Hartley, J. A.; Khan, N.; Souhami, R. L.; Mendonca, A. J.; Lown, J. W. *J. Photochem. Photobiol. B* **1992**, *15*, 317–335.
16. Warner, S. D.; Farant, J. P.; Butler, I. S. *Chemosphere* **2004**, *54*, 1207–1215.
17. Fu, P. P.; Heflich, R. H.; Von Tungeln, L. S.; Yang, D. T.; Fifer, E. K.; Beland, F. A. *Carcinogenesis* **1986**, *7*, 1819–1827.
18. Miller, D. W.; Evans, F. E.; Fu, P. P. *Spectros. Int. J.* **1985**, *4*, 91–94.
19. Serrano, M.; Hannon, G. J.; Beach, D. *Nature* **1993**, *366*, 704–707.
20. Oikawa, S.; Hirosawa, I.; Hirakawa, K.; Kawanishi, S. *Carcinogenesis* **2001**, *22*, 1239–1245.

Available online at www.sciencedirect.com
ScienceDirect
European Journal of Pharmacology 574 (2007) 192–200
www.elsevier.com/locate/ejphar

ME3738 protects against lithocholic acid-induced hepatotoxicity, which is associated with enhancement of biliary bile acid and cholesterol output

Masahiro Nomoto [a,b], Masaaki Miyata [a,*], Miki Shimada [a], Kouichi Yoshinari [a], Frank J Gonzalez [c], Shigeki Shibasaki [b], Tohru Kurosawa [b], Yasuhiro Shindo [b], Yasushi Yamazoe [a,d]

[a] *Division of Drug Metabolism and Molecular Toxicology, Graduate School of Pharmaceutical Sciences, Tohoku University, Aramaki, Aoba-ku, Sendai 980-8578, Japan*
[b] *Toxicology and Pharmacokinetics Research Labs., Pharmaceutical Research Center, Meiji Seika Kaisha, Ltd., Yokohama 222-8567, Japan*
[c] *Laboratory of Metabolism, National Cancer Institute, National Institutes of Health, Bethesda, Maryland 20892, USA*
[d] *CRESCENDO, The Tohoku University 21st Century "Center of Excellence" Program, Sendai 980-8578, Japan*

Received 17 April 2007; received in revised form 22 June 2007; accepted 4 July 2007
Available online 10 July 2007

Abstract

ME3738 (22β-methoxyolean-12-ene-3β, 24(4β)-diol), a derivative of soyasapogenol, attenuates liver disease in several models of chronic liver inflammation. In the present study, we have investigated a protective effect of ME3738 in a typical bile acid-induced cholestatic liver model, lithocholate (LCA) feeding mouse. Co-administration of ME3738 resulted in decreases in plasma alanine aminotransferase (ALT) and alkaline phosphatase (ALP) activities and hepatic bile acid level, and increases in biliary outputs of bile acid and cholesterol, as compared with the results in mice treated with LCA alone. LCA sulfation by hydroxysteroid sulfotransferase 2a and hydroxylation have been reported to be involved in protection against LCA-induced hepatotoxicity. ME3738-treatment, however, had no clear influence on the hydroxysteroid sulfotransferase 2a protein level and LCA 6α-, 6β- and 7α-hydroxylase activities, but increased biliary cholesterol output. Cholate (CA)-treatment has been shown to induce hepatotoxicity in farnesoid X receptor-null mice, which is scarcely dependent on bile acid sulfation and hydroxylation but associated with decreased biliary bile acid output. Co-administration of ME3738 decreased the ALT and ALP activities and hepatic bile acid level, and increased biliary outputs of bile acid and cholesterol in farnesoid X receptor-null mice, as compared with the results in the mice treated with CA. Moreover, a clear correlation between biliary outputs of cholesterol and bile acid was observed in these two bile acid-induced hepatotoxicity mouse models. These results suggest that ME3738 protects against bile acid-induced hepatotoxicity through increased biliary bile acid output that is not related to bile acid metabolism but associated with cholesterol output.

Keywords: ATP-binding cassette g5/8 (Abcg5/8); Bile salt export pump (Bsep, Abcb11); Cholesterol; Farnesoid X receptor (Fxr); Lithocholic acid

1. Introduction

ME3738 (22β-methoxyolean-12-ene-3β, 24(4β)-diol), a derivative of soyasapogenol, attenuates liver disease in several models of acute and chronic liver inflammation induced with acetaminophen, carbon tetrachloride and concanavalin A (Klein et al., 2003; Meiji Seika Kaisha, 2006; Kuzuhara et al., 2006). In the present study, we aimed to investigate a protective effect of ME3738 in a lithocholate (LCA)-induced cholestatic liver model.

LCA is a hydrophobic secondary bile acid and LCA feeding is known to cause intrahepatic cholestasis in mice (Yousef et al., 1997; Fickert et al., 2006). Furthermore, LCA is cytotoxic in rat primary hepatocytes and in human erythrocytes (Heuman et al., 1991). To elucidate the protective mechanisms of compounds against bile acid-induced hepatotoxicity, LCA is commonly used to prepare a hepatotoxicity model in experimental animals. Serum LCA concentration was higher in choronic hepatitis C patients and end-stage choronic liver disease patients than in healthy volunteers (Fischer et al., 1996; Jorquera et al., 2005), and the accumulation of LCA in circulating bile acids was thought to contribute to liver injury in patients (Carey et al., 1966). These reports suggest that LCA-induced cholestatic model represents clinical cholestatic patients. The mechanisms against LCA-induced hepatotoxicity, however, have not been completely elucidated yet.

* Corresponding author. Tel.: +81 22 795 6829; fax: +81 22 795 6826.
E-mail address: miyata@mail.pharm.tohoku.ac.jp (M. Miyata).

0014-2999/$ - see front matter © 2007 Elsevier B.V. All rights reserved.
doi:10.1016/j.ejphar.2007.07.004

A protective mechanism against LCA-induced hepatotoxicity has been reported to involve an enhancement in LCA sulfation by hydroxysteroid sulfotransferase 2a (Sonoda et al., 2002; Kitada et al., 2003) and hydroxylation (Xie et al., 2001; Hofmann, 2004). LCA and tauroLCA were good substrates of sulfation by hydroxysteroid sulfotransferase 2a. In particular, 3α-sulfated tauroLCA was excreted in feces easily, escaping from enterohepatic circulation (Miyata et al., 2006). Thus, oxidation and sulfation are likely to be the major protective mechanisms against LCA-induced hepatotoxicity.

In order to determine whether ME3738 protects against hepatotoxicity in another mouse model that is independent of bile acid metabolism, we chose a cholate (CA)-treated farnesoid X receptor-null mouse model. CA treatment has been shown to cause hepatotoxicity in farnesoid X receptor-null mice that are more susceptible to this treatment than wild-type mice, along with a decrease in the biliary bile acid output followed by an increase in the hepatic bile acid concentration (Sinal et al., 2000; Miyata et al., 2005).

In the present study, we investigated whether ME3738 protected against typical bile acid, LCA- and CA-induced hepatotoxicity and searched for its protective mechanism in these toxicities.

2. Materials and methods

2.1. Chemicals

ME3738 was synthesized at Meiji Seika Kaisha, Ltd. (Yokohama, Japan). Lithocholic acid (LCA), ursodeoxycholic acid (UDCA), cholic acid (CA), taurocholic acid (TCA), chenodeoxycholic acid (CDCA), taurochenodeoxycholic acid (TCDCA), deoxycholic acid (DCA), taurodeoxycholic acid (TDCA), and taurolithocholic acid (TLCA) were purchased from Sigma-Aldrich (St. Louis, MO). Hiodeoxycholic acid (HDCA), murideoxycholic acid (MDCA), β-muricholic acid (βMCA), tauro-β-muricholic acid (TβMCA), tauroursodeoxycholic acid (TUDCA), and 5β-cholanic acid 3α, 6β-diol (Internal standard for HPLC assay) were purchased from Steraloids (Newport, RI). L-column ODS (2.1 × 150 mm) was obtained from Chemicals Evaluation and Research Institute (Tokyo, Japan). Enzymepak 3α-HSD column was purchased from Jasco (Tokyo, Japan). ATP-binding cassette g8 polyclonal antibody was purchased from Novus biological, Inc (Littleton, CO).

2.2. Animal treatment and sample collection

C57BL/6N female mice (Charles River Japan Inc., Yokohama, Japan) and farnesoid X receptor-null mice (Sinal et al., 2000) were housed under standard 12 h light/12 h dark cycle. Before experiment, mice were fed standard diet CE-2 (Clea, Tokyo, Japan) and water ad libitum for acclimation. Experimental diets used were the mixture of 0.15 (w/w)% ME3738, 0.75% LCA, 0.75% LCA+0.05% ME3738 or 0.75% LCA+0.15% ME3738 with the standard diet. Nine- to eleven-week-old mice were used for the experiments. C57BL/6N mice were fed the experimental diets for 6 days. Farnesoid X receptor-null mice were fed a 0.25% CA or a 0.25% CA+0.15% ME3738 diet for 6 days. Blood and liver samples were taken for biochemical assays. Total RNA was prepared from the livers using the RNAgents total isolation system (Promega, Madison, WI), and RNA concentrations were determined by measuring absorbance at 260 nm using a DU800 spectrophotometer (Beckman Coulter, Fullerton, CA). Biliary excretion was monitored in mice anesthetized with diethyl ether. After ligation of the common bile duct, the gall bladder was cannulated with a polyethylene-10 tube (Becton Dickinson, Sparks, MD) with an internal diameter of 0.28 mm. The cannula was ligated into the gall bladder to obtain bile samples. After 5 min equilibration time, bile was collected for 30 min. The animals were treated humanely, and animal experiments were performed in accordance with the Guide for the Care and Use of Laboratory Animals as adopted and promulgated by the National Institutes of Health.

2.3. Plasma diagnosis parameters and plasma, hepatic or biliary lipids related parameters

Plasma alanine aminotransferase (ALT) activities were measured using a commercial kit, Transaminase CII-B-test Wako (Wako Pure Chemicals, Osaka, Japan). Plasma alkaline phosphatase (ALP) activity was measured using Alkaliphospha *B*-test Wako (Wako Pure Chemicals, Osaka, Japan). Hepatic and biliary bile acid, total cholesterol and phospholipid concentrations were measured using the total bile acid test Wako, cholesterol *E*-test Wako and Rinshishitsu *C*-test Wako, respectively (Wako Pure Chemicals, Osaka, Japan). Hepatic and biliary 3α-hydroxy bile acid concentrations were measured by HPLC as described previously (Kitada et al., 2003; Miyata et al., 2005).

Table 1
Sequence of primers for RT-PCR

Name	Cycle	Forward	Reverse	Amplicon size (bp)	Accession no.
Abcg5	30	CCTTGGTGGAACATCAAATC	TGATTTGCAGTCATGCAGTC	532	AF312713
Abcg8	35	AGCTTCAAAGTGAGGAGTGG	AAGGACCAGGTCAAATAGCC	578	AF324495
Bsep	28	ACAGCATTACAGCTCATTCAGAG	TCCATGCTCAAAGCCAATGATCA	423	AF133903
Mdr2	30	CTCGTTAACATGCAGACAGCAG	GACCAGGGAGAACATGTTACAC	371	NM008830
Gapdh	26	TGCATCCTGCACCACCAACTG	GTCCACCACCCTGTTGCTGTAG	531	NM008084

Abcg5: ATP-binding cassette g5; Abcg8: ATP-binding cassette g8; Bsep: Bile salt export pump; Mdr2: Multi-drug resistance protein 2; Gapdh: Glyceraldehyde-3-phosphate-dehydrogenase.

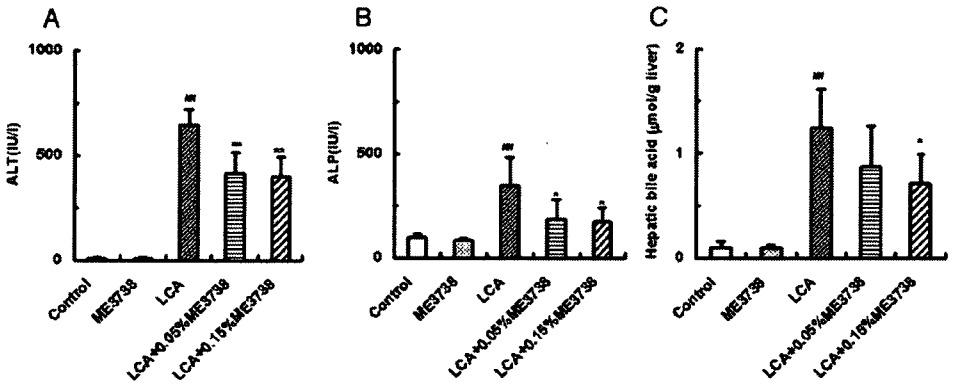

Fig. 1. Plasma alanine aminotransferase (ALT: A) and alkaline phosphatase (ALP: B) activities, and hepatic bile acid concentration (C). Plasma and liver homogenates were prepared from C57BL/6N mice fed a control, 0.15% ME3738, 0.75% LCA, LCA+0.05% ME3738 or LCA+0.15% ME3738 diet for 6 days. Plasma ALT and ALP activities, and hepatic bile acid concentration were measured by enzyme-colorimetric method. Data are shown as the mean±S.D. ($n=5$). ## Significantly different from control group ($P<0.01$). *,** Significantly different from LCA group ($P<0.05$, $P0.01$, respectively).

2.4. Immunoblot analysis

A bile salt export pump polyclonal antibody was prepared against the purified recombinant mouse bile salt export pump (Miyata et al., 2005). Hydroxysteroid sulfotransferase 2a polyclonal antibodies were prepared against the purified recombinant rat hydroxysteroid sulfotransferase 2a1 protein that reacts with mouse hydroxysteroid sulfotransferase 2a (Shimada et al., 2001). Plasma membrane and cytosolic proteins were prepared from the livers as described previously (Trauner et al., 1997). Plasma membrane for ATP-binding cassette g8 and bile salt export pump, and cytosolic proteins for hydroxysteroid sulfotransferase 2a were loaded onto a sodium dodecyl sulfate-polyacrylamide gel, isolated, and transferred to nitrocellulose membrane. The membranes were immunostained with ATP-binding cassette g8, bile salt export pump or hydroxysteroid sulfotransferase 2a1 polyclonal antibodies (1:1000 dilution), respectively. The membrane was washed five times with Tween 20 containing phosphate buffer, and incubated with phosphatase-conjugated goat anti-rabbit IgG (1: 3000 dilution), 5-bromo-4-chloro-3-indolylphosphate, and nitro blue tetrazonium as described previously (Honma et al., 2002). The stained membranes were scanned with an Epson GT-8700 scanner, and the band intensities were measured by use of the NIH image (version 1.59) software (Bethesda, MD).

2.5. LCA hydroxylase activities

LCA hydroxylase activities were measured using the method of Zimniak et al. with minor modifications (Zimniak et al., 1989). Four hundred and fifty μl of incubation mixture containing 0.1 mol/l potassium phosphate buffer (pH 7.4), 0.05 mmol/l EDTA, 2 mmol/l dithiothreitol, 2 mmol/l NADPH, and 0.5 mg microsomal protein/ml was gently mixed and pre-incubated for 5 min. The incubation at 37 °C was initiated by addition of 50 μl of 2 mmol/l LCA that was dissolved with 10% methanol containing potassium phosphate buffer. The incubation was terminated 30 min later by addition of 1 ml ethyl acetate

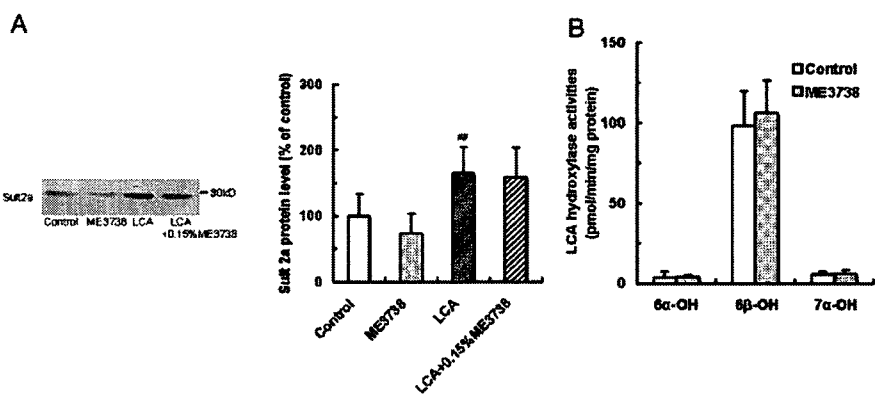

Fig. 2. Hepatic hydroxysteroid sulfotransferase 2a (Sult2a) protein levels and LCA hydroxylase activities. A) These protein levels were measured by Western blot analysis. Cytosolic protein was subjected to a sodium dodecyl sulfate-polyacrylamide gel and electrically transferred to nitrocellulose membranes for immuno-staining with anti-rat Sult2a1 antibodies. Data are shown as the mean±S.D. ($n=5$). B) The measurement of 6α-, 6β- and 7α-hydroxylation activities of LCA was described under Materials and methods. The concentrations of HDCA, MDCA and CDCA were measured by HPLC and these velocities were calculated. ## Significantly different from control group ($P<0.01$).

and rapid cooling. One hundred μl of 1 mol/l HCl and 2.5 μl of 0.4 mmol/l 5β-cholanic acid 3α, 6β-diol ethanol solution (Internal standard of HPLC) were added, and centrifuged at 2000 ×*g* for 10 min under 4 °C condition. The supernatant was collected and dried at 37 °C under N_2 gas, and then dissolved in 50% ethanol. The concentrations of HDCA, MDCA and CDCA were measured by HPLC and these velocities were calculated.

2.6. Analysis of mRNA levels

Messenger RNA (mRNA) levels of differentially expressed genes were analyzed using reverse transcription-polymerase chain reaction (RT-PCR). Single-strand cDNAs were constructed using an oligo (dT) primer with the Ready-to-Go You-Prime First-strand Beads kit (GE Healthcare UK Ltd, Buckinghamshire, UK). These cDNAs provided templates for PCRs using specific primers at a denaturation temperature of 94 °C for 30 s, an annealing temperature of 58 °C for 30 s, and an elongation temperature of 72 °C for 30 s in the presence of deoxynucleoside-5′-triphosphates and Taq polymerase. The PCR cycle numbers were titrated for each primer pair to ensure amplification in linear range. The reaction was completed by 7 min incubation at 72 °C. PCR products were analyzed in 2% agarose gel (w/v) containing ethidium bromide for visualization. The specific forward and reverse primers for the genes examined by PCR are shown in Table 1. These mRNA levels were normalized from Glyceraldehyde-3-phosphate-dehydrogenase (GAPDH) mRNA levels.

2.7. Statistical analysis

All data are shown as the mean ± S.D. Statistically significant differences among groups were assessed by ANOVA followed by Dunnet's multiple comparison with the SAS software (SAS Institute Inc., Cary, NC). Probability values of less than 0.05 were considered to be statistically significant.

3. Results

3.1. Influence of ME3738 administration on LCA-induced hepatotoxicity

Plasma alanine aminotransferase (ALT) and alkaline phosphatase (ALP) activities were increased to 643 and 349 IU/l, respectively, following LCA treatment, which suggested that severe hepatotoxicity and cholestasis were induced in the mice. In contrast, co-administration with 0.05 and 0.15% ME3738 significantly reduced LCA-induced ALT by 35 and 38% and ALP by 46 and 50%, respectively (Fig. 1A and B). As well as ALT and ALP activities, the hepatic bile acid concentration was increased in LCA-treated mice. The concentration in LCA-treated mice was approximately 13-fold higher than that in control mice (Fig. 1C). Co-administration with ME3738 reversed the elevation of concentrations, as compared with LCA-treated mice. These data indicate that ME3738 lowers the elevation of hepatic bile acid concentrations and protects against LCA-induced hepatotoxicity.

Table 2
Hepatic bile acid composition (A) and biliary bile acid output (B)

	βMCA	TβMCA	UDCA	TUDCA	CA	TCA	CDCA	TCDCA	DCA	TDCA	LCA	TLCA
(A) Liver concentration (μmol/g liver)												
Control	0.02±0.02 (0.18)	N.D.	N.D.	N.D.	N.D.	0.09±0.03 (0.82)	N.D.	N.D.	N.D.	N.D.	N.D.	N.D.
ME3738	0.01±0.01 (0.11)	N.D.	N.D.	N.D.	N.D.	0.08±0.02 (0.89)	N.D.	N.D.	N.D.	N.D.	N.D.	N.D.
LCA	N.D.	N.D.	N.D.	N.D.	N.D.	0.17±0.02 (0.14)	N.D.	0.23±0.09 (0.19)	N.D.	0.02±0.01 (0.02)	N.D.	0.82±0.31 (0.66)
LCA +0.05% ME3738	N.D.	N.D.	N.D.	N.D.	N.D.	0.13±0.05 (0.15)	N.D.	0.18±0.11 (0.21)	N.D.	0.01±0.01 (0.01)	N.D.	0.56±0.24 (0.64)
LCA +0.15% ME3738	N.D.	N.D.	N.D.	N.D.	N.D.	0.13±0.04 (0.18)	N.D.	0.16±0.06 (0.23)	N.D.	0.01±0.01 (0.01)	N.D.	0.42±0.21 (0.59)
(B) Biliary output (μmol/min/kgw)												
Control	N.D.	0.22±0.06 (0.11)	N.D.	0.02±0.00 (0.01)	N.D.	1.65±0.37 (0.86)	N.D.	0.01±0.00 (0.01)	N.D.	0.02±0.00 (0.01)	N.D.	N.D.
ME3738	N.D.	0.37±0.04 (0.11)	N.D.	0.04±0.01 (0.01)	N.D.	2.23±0.25 (0.83)	N.D.	0.02±0.00 (0.01)	N.D.	0.02±0.01 (0.01)	N.D.	N.D.
LCA	N.D.	0.17±0.10 (0.11)	N.D.	N.D.	N.D.	0.43±0.18 (0.27)	N.D.	0.69±0.21 (0.43)	N.D.	0.04±0.01 (0.03)	N.D.	0.25±0.05 (0.16)
LCA +0.05% ME3738	N.D.	0.15±0.08 (0.04)	N.D.	0.02±0.02 (0.01)	N.D.	1.22±0.73 (0.34)	N.D.	1.58±0.66 (0.44)	N.D.	0.02±0.01 (0.01)	N.D.	0.59±0.29 (0.16)
LCA +0.15% ME3738	N.D.	0.48±0.24 (0.10)	N.D.	N.D.	N.D.	1.14±0.74 (0.25)	N.D.	2.00±0.81 (0.43)	0.01±0.01 (0.00)	0.16±0.14 (0.03)	N.D.	0.80±0.46 (0.17)

Hepatic and biliary bile acid compositions were determined by HPLC. Liver homogenates were prepared and bile was collected from C57BL/6N mice fed a control, 0.15% ME3738, 0.75% LCA, LCA+0.05% ME3738 or LCA+0.15% ME3738 diet for 6 days. Data are shown as the mean±S.D. (n=5). N.D. of liver concentration and biliary output represents below 0.01 μmol/g liver and 0.01 μmol/min/kgw, respectively. Numbers in parenthesis represent % of the total bile acids. βMCA; β-Muricholate, TβMCA; Tauro-β-muricholate, UDCA; Ursodeoxycholate, TUDCA; Tauroursodeoxycholate, CA; Cholate, TCA; Taurocholate, CDCA; Chenodeoxycholate, TCDCA; Taurochenodeoxycholate, DCA; Deoxycholate, TDCA; Taurodeoxycholate, LCA; Lithocholate, TLCA; Taurolithocholate.

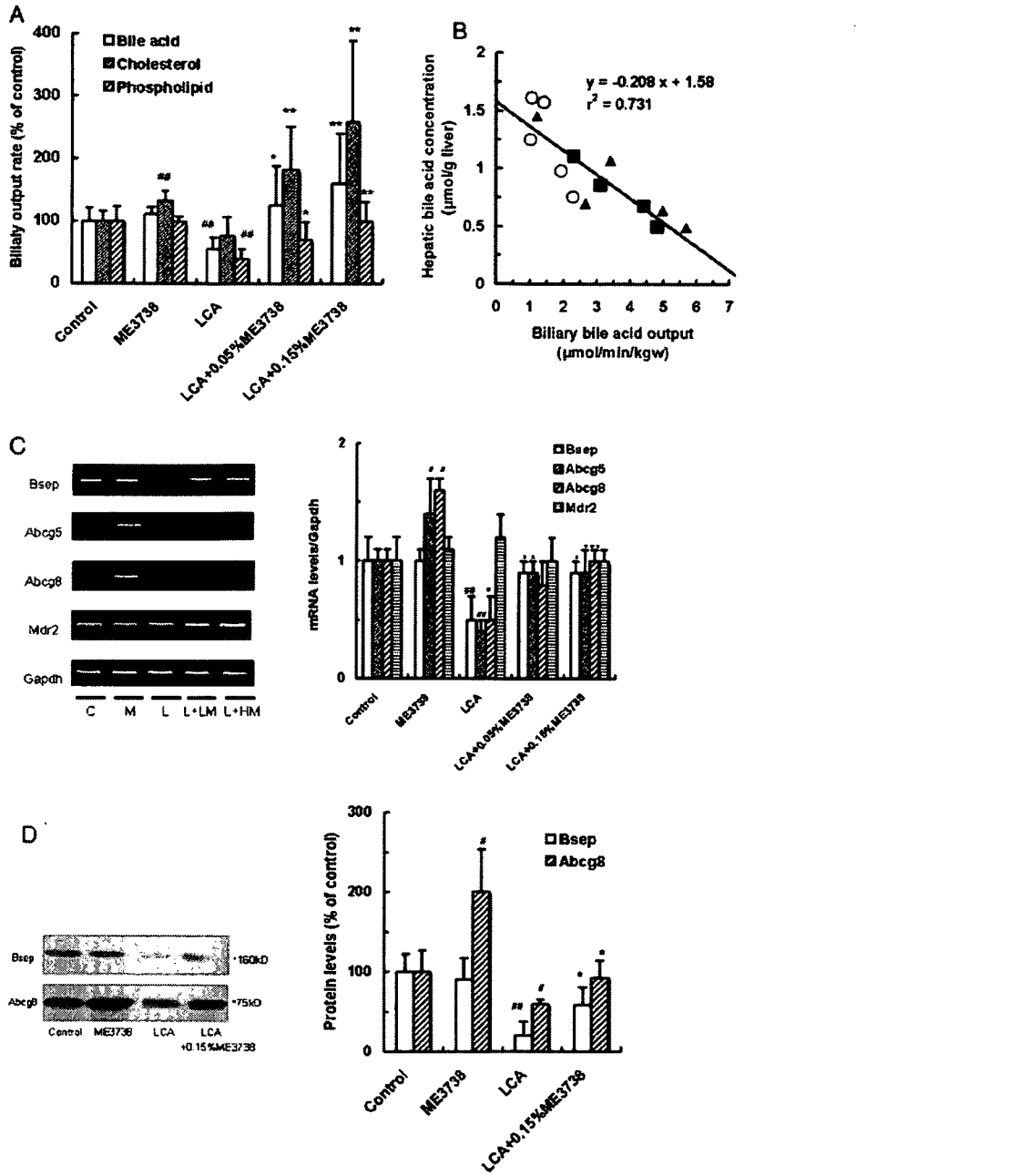

Fig. 3. Biliary bile acid, cholesterol and phospholipid outputs (A), correlation between biliary bile acid output and hepatic bile acid concentration (B), hepatic expression of transporter-related genes (C), and bile salt export pump (Bsep) and ATP-binding cassette g8 (Abcg8) protein levels (D). A) The bile was collected for 30 min by bile duct cannulation from C57BL/6N mice fed a control, 0.15% ME3738, 0.75% LCA, LCA+0.05% ME3738 or LCA+0.15% ME3738 diet for 6 days. Biliary bile acid, cholesterol and phospholipid concentrations were measured by enzyme-colorimetric method. B) Liver homogenate was prepared from C57BL/6N mice fed a 0.75% LCA (open circle), LCA+0.05% ME3738 (closed triangle) or LCA+0.15% ME3738 (closed square) diet for 6 days. The hepatic bile acid concentration was measured by enzyme-colorimetric method. C) Hepatic mRNAs were prepared from C57BL/6N mice fed a control (C), 0.15% ME3738 (M), 0.75% LCA (L), LCA+0.05% ME3738 (L+LM) or LCA+0.15% ME3738 (L+HM) diet for 6 days. The hepatic mRNA levels were measured by RT-PCR. Specific primers represented in Table 1. D) Bsep and Abcg8 protein levels were measured by Western blot analysis. Plasma membrane proteins were subjected to sodium dodecyl sulfate-polyacrylamide gels and electrically transferred to nitrocellulose membranes for immuno-staining with anti-mouse Bsep and anti-human Abcg8 antibody. Data are shown as the mean±S.D. ($n=4$). $^{\#}$, $^{\#\#}$ Significantly different from control group ($P<0.05$, $P<0.01$, respectively). *, ** Significantly different from LCA group ($P<0.05$, $P<0.01$, respectively).

3.2. Hepatic hydroxysteroid sulfotransferase 2a protein levels

LCA sulfation by hydroxysteroid sulfotransferase 2a has been reported to be involved in the protection against LCA-induced hepatotoxicity. The hepatic hydroxysteroid sulfotransferase 2a protein level, however, was not clearly different between control and ME3738-treated mice (Fig. 2A). The protein level increased by 1.7-fold in LCA-treated mice, as

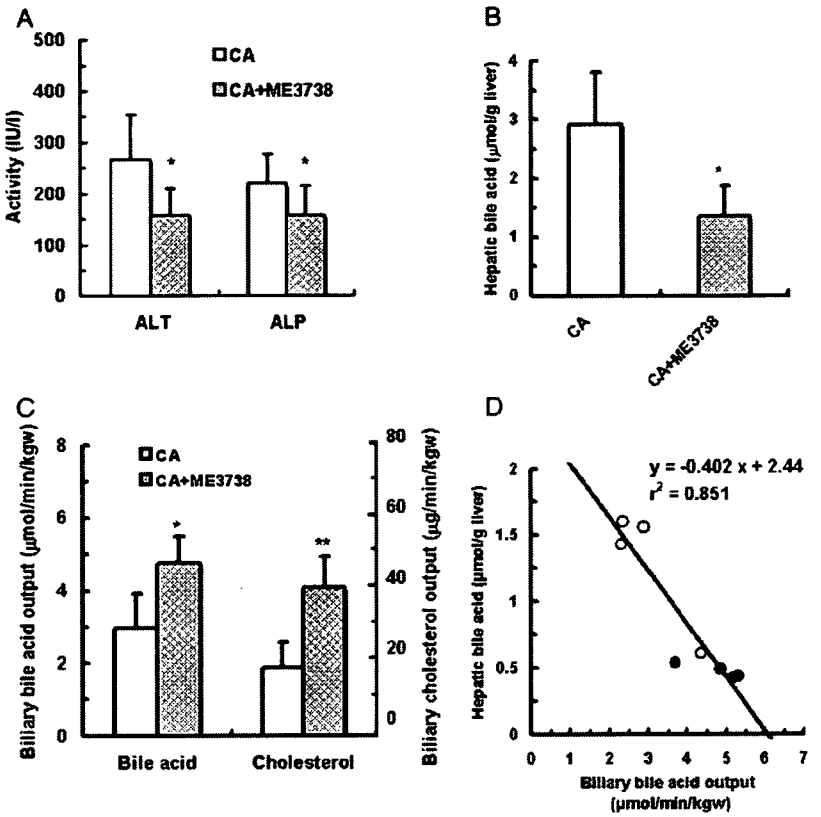

Fig. 4. Plasma alanine aminotransferase (ALT) and alkaline phosphatase (ALP) activities (A), hepatic bile acid level (B), biliary cholesterol and bile acid outputs (C), correlation between biliary bile acid output and hepatic bile acid concentration (D) in farnesoid X receptor-null mice fed a 0.25% cholate (CA) or CA+0.15% ME3738 diet. Plasma and liver homogenates were prepared from farnesoid X receptor-null mice fed a CA or CA+0.15% ME3738 diet for 6 days. A) Plasma ALT and ALP activities were measured by enzyme-colorimetric method. B) Hepatic bile acid concentration was measured by enzyme-colorimetric method. C) The bile was collected for 30 min by bile duct cannulation. Biliary bile acid and cholesterol concentrations were measured by enzyme-colorimetric method. D) Plots represent CA-treated mice (open circle) and CA+ME3738 treated mice (closed circle). Data are shown as the mean±S.D. (n=3–5). *,** Significantly different from the CA group ($P<0.05$, $P<0.01$, respectively).

compared with that in the control mice. No clear enhancement in the hepatic hydroxysteroid sulfotransferase 2a protein level was observed in mice co-treated with ME3738 and LCA, as compared with LCA-treated mice.

3.3. LCA hydroxylase activities

LCA is mainly oxidized to produce 6α-, 6β- and 7α-hydroxy derivatives (Zimniak et al., 1989). Therefore, 6α-, 6β- and 7α-hydroxylase activities of LCA were measured using liver microsomes prepared from the control and ME3738-treated C57BL/6N mice. The 6α-, 6β- and 7α-hydroxylase activities were not significantly different between the control and ME3738-treated mice (Fig. 2B). The 6β-hydroxylase activity was approximately 20- to 30-fold higher than 6α- and 7α-hydroxylase activities. This result is consistent with the data from Zimniak et al.

3.4. Hepatic and biliary bile acid composition

To determine the influence of ME3738 administration on bile acid composition, the hepatic and biliary bile acid levels were measured in mice that were fed a control diet or a diet supplemented with ME3738, LCA or LCA+ME3738. No obvious changes in hepatic and biliary bile acid compositions were observed in ME3738-treated mice, as compared with the control mice. Hepatic tauroLCA (TLCA), taurochenodeoxycholate (TCDCA) and taurocholate (TCA) concentrations were, however, increased in the LCA-treated mice, whereas ME3738 co-treatment reversed the increase in these bile acid levels in a dose-dependent manner (Table 2). Biliary TLCA, TCDCA and TCA outputs were decreased in LCA-treated mice, whereas ME3738 co-treatment retrieved the decrease in biliary bile acid output in a dose-dependent manner (Table 2). No obvious changes in hepatic and biliary bile acid compositions were also observed in LCA+ME3738-treated mice, as compared with LCA-treated mice.

3.5. Bile flow, and biliary bile acid, cholesterol and phospholipid output

We measured bile flow rate, initially. The bile flow rate in mice fed a control, ME3738, LCA, LCA+0.05% ME3738 or LCA+0.15% ME3738 diet was 94.2± 13.3, 95.7 ± 5.1, 52.9±

14.4, 101.4± 37.5 and 115.5± 20.3 μl/min/kgw, respectively. The rate was significantly decreased in LCA-treated mice, compared with that in control mice ($P<0.01$). Bile is known to consist mainly of bile acid, cholesterol and phospholipid. We therefore considered that the mechanism of hepatic bile acid reduction by ME3738 was involved in biliary outputs of bile acid, cholesterol and phospholipid. Their outputs were decreased in LCA-treated mice. In contrast, co-administration of ME3738 increased them (Fig. 3A). ME3738 administration alone resulted in an increase in biliary output of cholesterol but not increases in biliary bile acid and phospholipids outputs. Biliary output of cholesterol was enhanced by ME3738 administration alone by approximately 1.5-fold.

3.6. Inverse correlation between biliary bile acid output and hepatic bile acid concentration

Co-administration of ME3738 increased biliary bile acid output and decreased hepatic bile acid concentration in LCA-treated mice. Therefore, a correlation between biliary bile acid output and hepatic bile acid concentration was determined. A clear inverse correlation ($r^2=0.731$) between them was observed in LCA- and LCA+ME3738-treated mice (Fig. 3B).

3.7. Hepatic mRNA levels

Biliary excretion of bile acid, cholesterol and phospholipid is mediated by bile salt export pump, ATP-binding cassette g5/8 and multi-drug resistance protein 2 (Mdr2), respectively. To assess changes in these gene expressions, we measured the expression levels of these transporters by RT-PCR. Consistent with the biliary cholesterol output, hepatic ATP-binding cassette g5 and g8 mRNA levels were increased significantly by 1.4- and 1.6-fold, respectively, in ME3738-treated mice. In LCA-treated mice, hepatic ATP-binding cassette g5/8 and bile salt export pump mRNA levels were decreased, and no clear changes were detected in the multi-drug resistance protein 2 mRNA level. The hepatic ATP-binding cassette g5, g8 and bile salt export pump mRNA levels in LCA+0.15% ME3738-treated mice were 2.3-, 2.0- and 1.8-fold higher than those in LCA-treated mice, respectively (Fig. 3C).

3.8. Hepatic bile salt export pump and ATP-binding cassette g8 protein levels

The hepatic bile salt export pump and ATP-binding cassette g5/8 mRNA levels were increased in LCA+ME3738-treated mice, as compared to those in LCA-treated mice. Thus, the hepatic bile salt export pump and ATP-binding cassette g8 protein levels were also measured. The former one was not enhanced, whereas the latter one was increased significantly in ME3738-treated mice (Fig. 3D). The hepatic bile salt export pump and ATP-binding cassette g8 protein levels were reduced to 20 and 60% of the control in LCA-treated mice, respectively. In LCA+ME3738-treated mice, these protein levels were enhanced by 2.9- and 1.5-fold, respectively, as compared to those in LCA-treated mice.

3.9. Influence of ME3738 administration on cholate-treated farnesoid X receptor-null mice

In order to assess whether ME3738 protects against hepatotoxicity in another mouse model that is independent of bile acid metabolism, we chose the cholate (CA)-treated farnesoid X receptor-null mouse model.

Plasma ALT and ALP activities were increased to 266 and 220 IU/l, respectively, in CA-treated farnesoid X receptor-null mice. Co-treatment with ME3738 significantly decreased both activities to 158 IU/l (Fig. 4A). Consistent with plasma diagnosis parameters, hepatic bile acid concentrations in farnesoid X receptor-null mice that were co-treated with ME3738 were lower than those in the mice treated with CA (Fig. 4B). Bile flow rate in CA and CA+ME3738 treated farnesoid X receptor-null mice was 73.7± 21.8 and 94.6± 7.3 μl/min/kgw, respectively. Biliary outputs of bile acid and cholesterol were increased up to 1.6- and 2.2-fold, respectively, in CA+ME3738-treated farnesoid X receptor-null mice, as compared with those in CA-treated farnesoid X receptor-null mice (Fig. 4C). A clear inverse correlation ($r^2=0.851$) between biliary bile acid output and hepatic bile acid concentration (Fig. 4D) was observed.

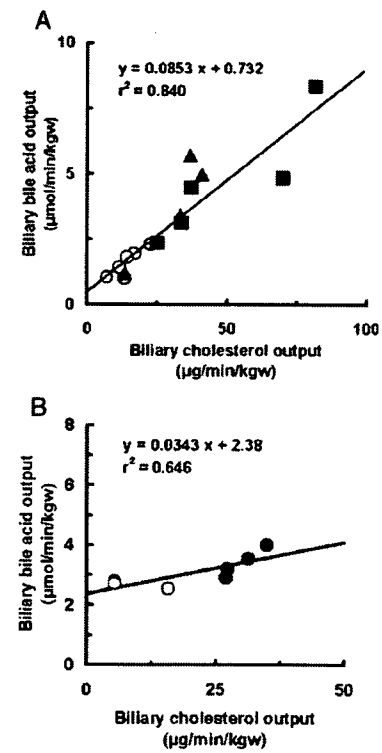

Fig. 5. Correlation between biliary outputs of cholesterol and bile acid. A) The bile was collected by bile duct cannulation from C57BL/6N mice fed a 0.75% LCA (open circle), LCA+0.05% ME3738 (closed triangle) or LCA+0.15% ME3738 (closed square) diet for 6 days. B) The bile was collected by bile duct cannulation from farnesoid X receptor-null mice fed a 0.25% CA (open circle) or CA+0.15% ME3738 (closed circle) diet for 6 days. Biliary bile acid and cholesterol concentrations were measured by enzyme-colorimetric method.